Quantitative measurement of tracer uptake in the lung in PET/CT

Garpered, Sabine

2020

Document Version:
Publisher's PDF, also known as Version of record

[Link to publication](#)

Citation for published version (APA):
Garpered, S. (2020). *Quantitative measurement of tracer uptake in the lung in PET/CT*. Lund University, Faculty of Medicine.

Total number of authors:
1

Quantitative measurement of tracer uptake in the lung in PET/CT

SABINE GARPERED

DEPT. OF CLINICAL PHYSIOLOGY AND NUCLEAR MEDICINE | LUND UNIVERSITY

Quantitative measurement of tracer uptake in the lung in PET/CT

Sabine Garpered

LUND
UNIVERSITY

Organization	Document name
LUND UNIVERSITY Faculty of Medicine	DOCTORAL DISSERTATION
Department of Translational Medicine Clinical Physiology and Nuclear Medicine, Malmö	**Date of issue** December 11 2020
Author Sabine Garpered	Sponsoring organization

Title and subtitle Quantitative measurement of tracer uptake in the lung in PET/CT

Abstract

Quantification is essential in Nuclear Medicine. The complexity of pulmonary tissue with regional variation of air, blood and tissue due to the effects of breathing results in inaccurate quantification of tracer uptake on the PET image. Different quantification approaches have been proposed. However, no standardized method exists for quantification in lung tissue accounting for the mentioned confounding factors. The overall aim of this thesis is to evaluate the impact of methods improving the quantification in lung tissue and differentiation between benign and malignant pulmonary nodules that account for air fraction and partial volume effect.

In **paper I** the aim was to examine whether current smokers have higher lung tissue uptake of ^{18}F-FDG than never-smokers when correcting for air fraction of the lungs. Sixty-six patients (33 never-smokers and 33 smokers) referred for a PET/CT were recruited for this study. There was a significant difference in activity concentration in lung tissue between never-smoker and current smoker only when normalizing for the air fraction.

In **paper II** the aim was to determine how the presence of intravenous (IV) contrast-enhanced CT influences SUV measurement corrected for both attenuation and air. Eighteen outpatients were referred with known malignancy other than lung cancer took part in the study. The results showed that only a marginal effect was seen in SUV between non-enhanced and IV contrast-enhanced CT when the air fraction was accounted for.

In **paper III** the aim was to evaluate the impact of a new practical method for quantification of mass, M_{PN}, and total metabolic activity, TLG_{PN}, in small pulmonary nodules. We selected 38 patients with pulmonary nodules (range 5-23mm) who underwent ^{18}F-FDG-PET/CT during 2009-2015 and 2017-2018. The results showed that correcting for the partial volume effect using TLG_{PN} and M_{PN} with this method may be more practical in clinical settings than the traditional volumetric parameters.

Paper IV describes the impact of the same method as in paper III on the volumetric parameters TLG_{PN}, and mass, M_{PN} in small pulmonary lesions, using respiratory gated, FDG-PET/CT and ungated FDG-PET/CT acquisition. Twenty-seven patients referred for PET/CT with suspicious pulmonary malignancy less than 23 mm in the lower and middle lobes were included in the study. Both ungated and gated FDG-PET/CT acquisitions showed similar values in TLG_{PN} measurements.

In conclusion, our approaches accounting for the confounding effects may improve the estimates of lung cell tracer concentration. These methods provide opportunities for pathophysiological research, studies of the relation between inflammation and biomarkers in the blood as well as reduction of lung function. Finally, the contribution to its nonvendor-specific feasibility may facilitate the use in clinical settings

Key words Lung density, IV contrast-enhanced FDG-PET/CT, partial volume effect, pulmonary nodules, respiratory motion, respiratory gated PET/CT acquisition

Classification system and/or index terms (if any)

Supplementary bibliographical information	**Language** English
ISSN 1652-8220	**ISBN** 978-91-7619-995-4

Recipient's notes	**Number of pages** 66	Price
	Security classification	

Signature *Sabine Garpered* Date 2020-11-05

Quantitative measurement of tracer uptake in the lung in PET/CT

Sabine Garpered

LUND
UNIVERSITY

Whatever you can do or dream you can, begin it.
Boldness has genius, power, and magic in it.
As soon as you trust yourself, you will know how to live.
Knowing is not enough; we must apply. Willing is not enough; we must do.
Correction does much, but encouragement does more.
Magic is believing in yourself; if you can do that, you can make anything happen.
All the knowledge I possess everyone else can acquire, but my heart is all my own

- Johann Wolfgang von Goethe (valda delar)

Table of Contents

List of papers

This thesis is based on the following papers, which will be referred to the text by their Roman numerals.

I. **Sabine Garpered**, David Minarik, Sandra Diaz, Lars Edenbrandt, Sven Valind, Per Wollmer: *Measurement of airway inflammation in current smokers by positron emission tomography*
(Clinical Physiology and Functional Imaging doi.org/10.1111/cpf.12590, 6 July 2019)

II. **Sabine Garpered**, David Minarik, Sven Valind, Sophia Frantz, Per Wollmer *Evaluation of ^{18}FDG uptake in lung parenchyma compensating for lung density: Comparison between non-enhanced low dose CT and intravenous contrast-enhanced diagnostic CT*
(Nuklearmedizin doi: 10.1055/a-1038-9933, 25 november 2019)

III. **Sabine Garpered**, David Minarik, Sophia Frantz, Ylva Gårdinger, Mariana Reza Felix, Sven Valin, Per Wollmer: *Quantification of pulmonary nodule mass and FDG uptake – a new and practical method.* In manuscript

IV. **Sabine Garpered**, David Minarik, Sophia Frantz, Sven Valind, Per Wollmer: *Comparison of respiratory gated and ungated FDG-PET/CT in FDG avid lung lesions: quantification with a novel practical method* In manuscript

Abstract

Quantification is essential in Nuclear Medicine. The complexity of pulmonary tissue with regional variation of air, blood and tissue due to the effects of breathing results in inaccurate quantification of tracer uptake on the PET image. Different quantification approaches have been proposed. However, no standardized method exists for quantification in lung tissue accounting for the mentioned confounding factors. The overall aim of this thesis is to evaluate the impact of methods improving the quantification in lung tissue and differentiation between benign and malignant pulmonary nodules accounting for air fraction and partial volume effect.

In paper I the aim was to examine whether current smokers have higher lung tissue uptake of ^{18}F-FDG than never-smokers when correcting for air fraction of the lungs. Sixty-six patients (33 never-smokers and 33 smokers) referred for a PET/CT were recruited for this study. There was a significant difference in activity concentration in lung tissue between never-smoker and current smoker only when normalizing for the air fraction.

In paper II the aim was to determine how the presence of intravenous contrast-enhanced CT influences SUV measurement corrected for both attenuation and air. Eighteen outpatients were referred with known malignancy other than lung cancer took part in the study. The results showed that only a marginal effect was seen in SUV between non-enhanced and IV contrast-enhanced CT when the air fraction was accounted for.

In paper III the aim was to evaluate the impact of a new practical method for quantification of mass, M_{PN} and total metabolic activity, TLG_{PN} in small pulmonary nodules. We selected 38 patients with pulmonary nodules (range 5-23mm) who underwent ^{18}F-FDG-PET during 2009-2015 and 2017-2018. The results showed that our method for quantification of mass and TLG of pulmonary nodules may be more practical in clinical settings than the traditional method/methods used for volumetric parameters.

Paper IV describes the impact of the same method as in paper III on the volumetric parameters TLG_{PN} in small pulmonary lesions, using respiratory gated FDG-PET/CT and ungated FDG-PET/CT acquisition. Twenty-seven patients referred for PET/CT with suspicious pulmonary malignancy less than 23 mm in the lower and middle lobes were included in the study. Both ungated and gated FDG-PET/CT acquisitions showed similar values in TLG_{PN} measurements.

In conclusion, our approaches accounting for the confounding effects may improve the estimates of lung cell tracer concentration. These methods provide opportunities for pathophysiological research, studies of the relation between inflammation and biomarkers in the blood as well as reduction of lung function. Finally, the contribution to its non-vendor specific feasibility may facilitate the use in clinical settings.

Populärvetenskaplig sammanfattning

PET/CT, positronemissionstomografi i kombination med CT är en bildgivande nuklearmedicinsk metod, som används i klinisk rutin sedan många år. Metoden har blivit ett alltmer betydelsefullt verktyg inom främst cancerdiagnostik tack vare dess förmåga att återge förändringar på cellnivå. Sådana förändringar uppstår innan strukturella förändringar kan ses med enbart CT. Tidig upptäckt av cancer är ofta viktigt för bästa behandlingsresultat. PET/CT används idag både för att upptäcka cancer och hitta spridning av redan känd cancer. Det används också för att utvärdera svar på cancer-behandling samt vid dosplanering inför strålbehandling. Vid en undersökning med PET/CT ges en injektion av radioaktivt märkta spårsubstanser. Den vanligaste substansen är en glukosanalog (en molekyl väldigt lik socker), som märks med radioaktivt fluor (^{18}F-FDG). Cancerceller använder mestadels glukos som sin viktigaste energikälla. Dessa celler har också en högre koncentration av glukostransportörer, vilka transporterar ^{18}F-FDG in i cellen. Detta för att kompensera det ökade behovet av glukos viket avspeglar sig som en förhöjd koncentration av FDG. Produkten ^{18}F-FDG-fosfat kvarstannar därefter i cellen, och kan fångas på bild av PET-kameran, samtidigt som CT ger en bild av var det ökade glukosbehovet finns.

PET/CT vid lungsjukdomar

Lungsjukdomar är en signifikant global hälsobörda som drabbar miljontals människor och där en stor del utgörs av kroniskt obstruktiv lungsjukdom, KOL. Behandlingsmöjligheterna är tyvärr fortsatt begränsade på grund av otillräcklig kunskap om de bakomliggande mekanismer som leder till utveckling och progress av sjukdomarna. Det är allmänt känt att inflammatoriska härdar i lungvävnaden har en förhöjd glukosomsättning. Tidiga studier har visat en ökad ansamling av FDG i de vita blodkropparna i lungorna vid induktion av inflammation [1-3]. Detta ger oss möjlighet till att hitta olika inflammatoriska tillstånd i lungorna, men kan också bidra med svårigheter vid undersökning av lungorna, t ex mycket lokala lunginflammationer eller tuberkulos som då kan misstas för lungcancer. Redan 1988 (Pantin et al) beskrevs att upptaget av FDG var ökat hos patienter med inflammation i lungans minsta enheter, alveolerna (alveolit). FDG-PET har också använts för bedömning av sjukdomsaktivitet och värdering av behandlingseffekt. Mätning av FDG har visat sig vara en mycket känslig metod för studier av låggradig inflammatorisk aktivitet i lungorna som vid kronisk obstruktiv lungsjukdom och där inflammationsprocessen i de små luftvägarna anses vara en viktig mekanism vid utveckling av kronisk obstruktiv lungsjukdom, KOL

Även hos rökare med normal lungfunktion har en ökad halt av vita blodkroppar noterats i de mindre luftvägarnas slem/vätska. KOL som till största delen är relaterad till tobakskonsumtion är ett samlingsbegrepp för inflammatoriska

förändringar i de små luftvägarna, bronkiolit och emfysem (ökat luftinnehåll i lungorna på grund av destruktion av lungvävnaden). Tillståndet är irreversibelt och resulterar i en låggradig kronisk inflammation. Vi vet också att KOL ökar risken för utveckling av lungcancer. I båda fallen har sjukdomsförloppen gått långt innan de båda sjukdomarna gör sig märkbara genom symtom och nedsatta lungfunktionstester.

Kvantifiering av lungvävnaden och enstaka lungförändrigar

Upptaget av ^{18}F-FDG eller aktivitetskoncentrationen är ett mått på glukos-konsumtionen i vävnaderna och benämns standardiserat upptagsvärde, SUV, som normaliseras till patientens vikt och injicerad mängd radioaktivitet. Denna antar att glukoskoncentrationen i kroppen är homogent fördelad och antar 1 g/mL. Detta gäller dock inte för lungvävnaden. Studier har nämligen visat att koncentrationen ligger runt 0,3 g/mL, på grund av lungvävnaden heterogena sammansättning, av en stor mängd luft och blod.

Lungtätheten varierar mycket med andningen och kroppens läge vilket försvårar mätning av aktivitetskoncentrationen i lungorna. I den kliniska vardagen tas ingen hänsyn till detta, vilket kan påverka bedömningen av SUV-värdet, framför allt i enstaka små lungförändringar där aktivitetskoncentrationen kan underskattas. Faktorer som ytterligare påverkar SUV-värdet utöver andningsrörelsen är biologiskt och fysikaliskt relaterade.

I denna avhandling evalueras en beräkningsmodell för en bättre diagnostik gällande små förändringars totala glukosmetabolism/aktivitetsupptag och massa, vilken tar hänsyn till den varierande lungtätheten genom korrektion av den stora mängden luft i lungvävnaden och andningsrörelse. Modellen möjliggör även en säkrare avgränsning av små lungförändringar som krävs för beräkning av det totala aktivitetsupptaget i dessa.

I delarbetena ingick patienter som var planerade för PET/CT undersökning av lungorna med frågeställningarna: diagnostik och stadieindelning. Patienter under radio-kemo terapeutisk behandling exkluderades för att undvika cytostatikans samt strålbehandlingens påverkan av SUV-värdet såsom strålinducerad lunginflammation, aktiv fibrosbildning samt reaktiv respons på cytostatika. I första delarbetet uteslöts patienter med känd lungsjukdom då dessa kan påverka aktivitetsupptaget och ge falskt förhöjda värden. Bildanalys och kvantifiering av lungtäthet och aktivitetskoncentration i vardera lunga gjordes i Matlab, specialkonstruerat mjukvaruprogram och i NM-fusion (Sectra Imaging IT Linköping).

I **delarbete I** såg vi en signifikant skillnad i aktivitetskoncentration i lungvävnaden mellan rökare och icke rökare endast då vi korrigerade för luftinnehållet

I **delarbete II** fann vi en marginell skillnad avseende aktivitetskoncentrationen i lungvävnaden i PET bilden vid attenueringskorrektion med lågdos CT och diagnostisk CT med i.v. kontrast när hänsyn togs till lungtätheten.

I **delarbete III** evaluerades en ny metod för att på ett enklare sätt kvantifiera det totala metabola aktivitetsupptaget och massa i enstaka små lungförändringar och samtidigt korrigera för den partiella volymseffekten (kamerans upplösningsförmåga, positronens räckvidd). Vi fann att denna metod är oberoende av användare i jämförelse med de andra beskrivna metoderna.

I **delarbete IV** jämförs den konventionella statiska bildtagningen med den andningsstyrda bildtagningen med PET med samma metod som i delarbete III. Vi fann ingen signifikant skillnad mellan dessa två bildtagningar avseende den totala metabola aktiviteten i små lungförändringar.

Abbreviations and terms

AC	Attenuation correction
AFC	Air fraction correction
AUC	Area under the curve
BPL	Bayesian penalized likelihood
COPD	Chronic obstructive pulmonary disease
$avHU_{BG}$	Average HU in a background region
$avHU_{CT}$	Average HU in a VVOI,CT
$avHU_{PN}$	Average HU in a PN
$avSUV_{VOI,PET}$	Average SUV in a VOI in the PET image
$avSUV_{PN}$	Average SUV in a PN
CI	Confidence interval
CT	Computer tomography
D	Density
FOV	Field of view
^{18}F-FDG	Fluoro-deoxyglucose labelled with 18F
GTV	Gross Tumor Volume
HU	Hounsfield units
ICC	Intraclass coefficient
i.v. $ceCTV_{PN}$	Intravenous contrast-enhanced CT
LOR	Line of response
M_{blob}	Mass of blob
$refM_{blob}$	Mass of reference blob
M_{PN}	Mass of a PN
MRT	Magnetic resonance tomography
NEMA	National Electric Manufacturers Association
OSEM	Ordered subset expectation maximisation
PACS	Picture archiving and communication system

PET/CT	Positron emission tomography combined with computed tomography
PN	Pulmonary nodule
PSF	Point spread function
PVE	Partial volume effect
ROC	Receiver Operating Curve
SiPM	Silicon photomultiplier
SUV	Standardised uptake value
SUV_{BG}	SUV of background tissue
SUV_{max}	Maximal SUV in a VOI
SUV_{PN}	SUV of a PN
TFE	Tissue fraction effect
TLG	Total lesion glycolysis
TLG_{PN}	TLG of a PN
TNM	Tumour, Node Metastasis
V	Volume
V_a	Voxel fractional air volume
V_{PN}	Volume of a PN
V_t	Voxel fractional tissue volume
VOI	Volume of interest
$V_{VOI,CT}$	Volume of a VOI in the CT image
$V_{VOI,PET}$	Volume of a VOI in the PET image

Introduction

The main subject of this research is to evaluate and attempt to provide an approach for the most significant issue associated with quantitative static PET parameter estimates in pulmonary tissue and in small pulmonary lesion.

Millions of people are affected by respiratory diseases, particular in chronic obstructive pulmonary disease, COPD, leading to a significant health burden globally which also is a risk factor for lung cancer [4]. Treatment options for COPD still remain limited because of the current insufficient knowledge of the underlying mechanisms that lead to the development and progression of respiratory diseases. Current conventional clinical measures, such as global lung function, computer tomography, magnetic resonance tomography, MRT and MRT with hyperpolarized helium gas (^{3}He) or with ^{129}Xe reflect disease severity rather than disease activity. Respiratory diseases are commonly associated with inflammation and a robust biomarker might aid the development of effective therapies and being useful in early-phase pharmacodynamic studies as a complement to other structural and pulmonary function test [5].To overcome the limitations and understand the associated molecular changes, non-invasive imaging techniques such as PET with ^{18}F-FDG PET imaging being the most studied and explored as a biomarker. Several studies have shown that PET/CT is able to identify inflammation and disease progression faster than conventional techniques. With this knowledge ^{18}F-FDG PET has been widely used as a biomarker in pulmonary inflammation [6-12].

The quantification with PET parameters in pulmonary tissue as well as nodules remains challenging because of the respiratory motion and variations of components such as tissue, air, blood, and water fractions within the lungs [13, 14], namely lung density. The proportions of these components further differ depending on the lung disease [6, 15-17]. Therefore, different quantification approaches have been developed to address these variabilities. However, no standardized approach has been proposed to date.

In this thesis a feasibility study has been performed using an improved analysis methodology to determine if more robust parameter estimates can be derived in the lung tissue and lung lesions. The new methodology was performed in a phantom study before applying to patients who had undergone static PET/CT studies with ^{18}F-FDG.

Background

Positron emission tomography, (PET) is a non-invasive imaging technique that uses different molecules labelled with radiotracers to image physiological and molecular tissue function, identifying changes at the cellular level most commonly used in oncology [18]. PET/CT scanners did not appear in the clinic until 2001 [19]. The main advantages of the multi-modality system is that it allows both anatomical and functional information in one clinic session.

Figure 1. New generation PET/CT system Discovery MI (GE Healthcare Milwaukee,WI, USA)

PET is also used in cardiology, neurology, and for imaging, different lung conditions [10, 11, 20, 21]. The systems consist of two scanners in one gantry with a shared patient bed (Figure 1). The advantages of this multi-modality system are the determination of both functional and anatomical information in one session and allows a fast attenuation acquisition for correction of the PET images compared to the earlier used correction with the time-consuming [68]Germanium acquisition. This is known as image fusion or co-registration.

The most common PET radiotracer is fluorine-18 labelled deoxyglucose (^{18}F-FDG) used for imaging glucose metabolism. It is a glucose analogue and is transported into cells by glucose transporter molecules and undergoes phosphorylation but is not metabolized further because it is missing a hydroxyl-group and will trapped in the cell. Because most of the tumour cells have increased metabolism of glucose, FDG uptake at a rate of 20 times as high as cells of noncancerous tissues results in a differentiation of tumour from surrounding normal cells. There are many other tracers mimicking naturally occurring substances in the body and are chosen dependent on the target of interest. Elevated FDG uptake are also seen in physiologic processes such as brain tissue, active muscles tissue, brown adipose tissue and with ongoing inflammatory processes, which complicates the detection of hyper metabolic tumours. FDG-PET can thus not reliably differentiate benign from malignant tissue in particular slowly growing tumours with a metabolism similar to normal tissues.

Table 1 shows a list of most commonly used radiotracers and their characteristics.

Table 1 (Cal-Gonzalez et al., 2013).

Isotope	Half Life	Mean Energy (keV)	Mean Positron Range in Water (mm)	Mean Positron Range in Lung (mm)
[18]F	109.8	249.8	0.64	2.14
[11]C	20.4	385.6	1.03	3.45
[13]N	10.0	491.8	1.32	4.43
[15]O	2.0	735.3	2.01	6.73
[68]Ga	67.7	352.6	2.24	7.41
[82]Rb	1.3	1168	4.29	13.90

Principle of positron emission tomography

PET imaging produces functional images by using radiotracers with a non-stable radioactive isotope that decays by emitting a particle called positron, a positively charged electron. The radiation emitted from an intravenously injected radiopharmaceutical is registered by multiple external detectors positioned at different orientations.

According to the carrier molecule, the isotope distributes within the tissues and emits a positron. The positron travels few mm, losing energy and interacts within a free electron in the tissue. An annihilation reaction occurs resulting in two photons with a high energy of 511 keV at almost exactly 180º from another and hits the PET scanner scintillator crystals and release detectable light bursts. The photon detection and the distribution are quantified and translated for image reconstruction, and visualizing the tracer uptake in the tissue [22].

If the two photons are traveling in straight lines, line of response, LOR without any interaction in the patient, they will be detected. This represents a so called *true coincidence.* To get a coincidence, the events must take place within a short time interval (nanoseconds) and the energy of both gamma rays must be approximately 511 keV [23]. The PET scanners can detect millions of coincidence events in a single examination [24].

However, a large fraction of the photons will either be absorbed or undergo scatter. The scattered photon has a lower energy but will not be disqualified by the system when it is detected together with its companion photon, representing *scatter coincidence*. False coincidence, *randoms,* appear when two photons are detected within the timing window and their true companion is lost to the system. (Figure 2)

Multiple rings of detectors inside the PET system record emission from the radiotracer. The distribution of the radioactivity, i.e. the PET image, is generated by different filter and reconstruction methods. The direction of the annihilation photons provides the location of the origin of the photons and the radioactive decay process that resulted in their emission, Figure 2.
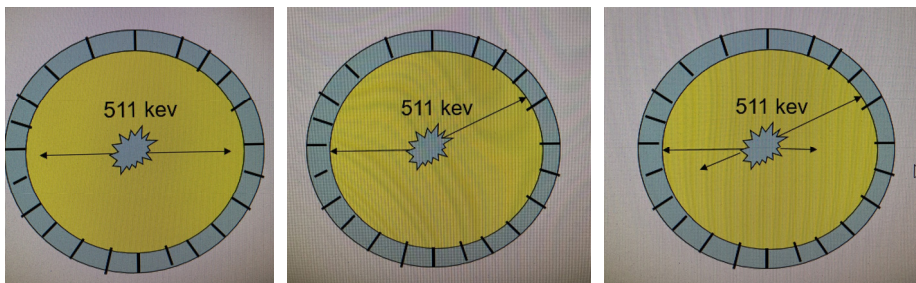
Figure 2. Line of response LOR true coincidence, scatter and randoms.

Attenuation correction and reconstruction

Correction must be applied for these different types of coincidence to overcome quantitative imaging errors. The main process of attenuation in the tissue is the Compton effect, scattering. One of the most important correction is the AC used for correction of the missing photons and correction of scatter and removes those

photons that are allocated incorrectly to LOR. These two correction methods can induce artefacts in the images. The reconstruction of the raw PET data into tomographic images can be done by different models/algorithms. The result of the reconstruction [25-29] (ToF, Q.Clear) depends on the matrix sizes, filtering and iterative methods [30, 31].

Computerised Tomography

The CT scanner gives anatomical information by a rotating X-ray source to build up 3D images. This is achieved by measurement of attenuation through a plane of the body with a limited thickness. The attenuation is dependent on the tissue density and X-ray energy. The attenuation values, known as Hounsfield Units, HU, are then converted to produce images [32]. The energy produced by the CT scanner of 60-120 keV differs from the energy in the PET (511 keV) and a specific conversion has to be done using a bi- or trilinear scaling model (water, air, soft tissue) [33, 34]. Tissues and material with much higher attenuation values e.g. metallic implants and contrast agents can cause image artefacts resulting in falsely high SUV values.

PET imaging acquisition

In static imaging the patient is injected with a weight adjusted radiotracer and then left to rest so that the tracer distribution in the whole body reaches an equilibrium, referred to uptake time (approximately 45-60 minutes). The patient is then placed on a scanner table that slides between the CT and PET camera. Due to the limited FOV the patient is moved through the scanner and the acquisition repeated to build up an image of the whole body, referred to as a bed position, which last 2-3 minutes per bed position [35].

Another imaging technique is the dynamic acquisition, mainly used in research. The acquisition begins immediately after the radiotracer injection while the patient lie on the scanner. The scanning can last 1-2 hours. This technique gives information about the change in radiotracer concentration observed over time within the body. Dynamic imaging is assessed using different kinetic analysis models.

Quantification of PET imaging

The advantage of PET compared to other nuclear medicine imaging techniques is the possibility to determine the absolute activity concentration. Thus the image can give information about activity concentration or SUV. Visual and qualitative criteria have been developed to facilitate the assessment of treatment response in tumours [36, 37].

Quantitative measurements of FDG uptake have shown promising results for assessment of disease activity in many cancers [38]. Measurements of SUV in combination with the visual evaluation is the most commonly used method in clinical practice due to its convenience. However, it is widely known that SUV measurements are affected by multiple biological, physical and technical factors. Knowledge of these confounding factors is essential for optimal evaluation of patients with cancer. Measuring the SUV requires an interactive workstation or a built-in measurement tool e.g. patient archive communication system, PACS.

Methods of FDG uptake assessment

Qualitative interpretation of FDG uptake is based on visual evaluation of images, where the target lesion is compared with normal FDG uptake in the surrounding background or with the FDG uptake in the mediastinal blood pool or the liver. The accuracy of the visual interpretation depends much on the reader`s knowledge of the normal physiology of FDG distribution, artefacts, tumour biology, post-therapy changes and experience [38].

Measurement of SUV is a semiquantitative approach which reflects the degree of radiotracer concentration in a lesion. It is defined as a ratio of radioactivity concentration in tissue C_t at a certain time, normalised to injected activity, A, and patient weight, W, by the formula

$$SUV = \frac{C_t}{A\,W}$$

where the SUV is measured in grams per millilitre, tissue tracer activity is in the kilobecquerels per millilitre, the injected dose in kilobequerels and patient weight in grams. The measurements are done by drawing a ROI and a VOI surrounding the target lesion or area of interest. The SUV_{max} is the most commonly reported parameters in clinical practice because it is simple and vendor independent. SUV_{max} represents the maximum voxel value in a region of interest and thus not the whole tumour metabolic burden in a non-homogenous tumour. Another disadvantage with SUV_{max} is the sensitivity to image noise, motion, patient characteristics and imaging parameters (reconstruction algorithm) [39].

Peak SUV is a hybrid value which is the mean value of radiotracer within a small fixed-sized region of interest surrounding the pixel with the highest activity and combines the reproducibility of SUV_{max} and decreases the noise. [38]. The disadvantage with this measure is its reduced accuracy in assessment of small lesions and shape of the lesion [35].

Multiple-Time-Point Imaging

Delayed time-point imaging is a concept were the patient is rescanned at different time points usually 2 or 3 hours after the standard scan, 60 minutes [40]. This concept is based on the observed increase of FDG uptake with time in malignant cells until 3 to 4 hours after injection [41, 42], whereas the FDG uptake decreases or stays the same in inflammatory or infectious diseases. However the clinical use of this concept remains controversial because large studies have shown an overlap of FDG uptake between benign and malignant lesions in dual time-point images [43].

Volumetric PET parameters

These parameters consist of metabolic tumour volume, MTV, and the total lesion glycolysis, TLG. MTV represents the volume of the tumour with FDG uptake. It is the volume inside a user- or algorithm-defined boundary that surrounds the metabolically active tumour. The TLG is calculated by multiplying the SUV_{mean} of the tumour and the MTV and represents both the size and the extent of FDG uptake [38]. MTV and TLG are considered to be more comprehensive and better to reflect the metabolic tumour burden. Several studies have shown that these two parameters correlate with risk stratification in different types of malignancies. Patients with higher MTV and TLG demonstrate a greater risk for local or regional recurrence, progression and higher mortality. There are also some evidence that the volumetric parameters are more sensitive in prediction of prognosis and treatment responses for patients with different malignancies [44-48]. However MTV and TLG have not been used in the clinical practice yet because the volumetric measurements require an accurate segmentation of the tumour, unlike SUV_{max}, and the optimal segmentation method to measure these values has not been established [39]. They are also significantly affected by the segmentation methods [49]. Tumour delineation using FDG PET image has also been used for radiotherapy treatment planning [50]. CT is the standard imaging for defining gross target volume, GTV, for radiotherapy in lung cancer. Several studies have shown that FDG PET-based MTV showed a lower inter-observer variability than CT-based GTV [51]. To determine the boundaries of the ROI/VOI multiple segmentation methods such as threshold-based or algorithm-based methods have been proposed and evaluated. The fixed absolute thresholds are commonly used for measuring MTV, with the most commonly used and accepted threshold of SUV 2.5 [52].

Factors affecting the quantification in thorax

The quantification of SUV is subject to many sources of variability from technical, physics-related and biologic-physiologic factors.

Some of the *technical errors* are for example the quality of FDG administration, scanner variability (different PET/CT scanners have different image reconstruction algorithm and acquisition parameters) and PVE caused by limited spatial resolution of the PET system. As aforementioned SUV measurements are highly dependent on the drawn ROI because in a 2-dimensional ROI one can miss the highest intensity voxel and a 3-dimensional ROI can include an adjacent FDG avid part of another tissue.

Contrast-enhanced CT with oral or intravenous agents can not only improve lesion localisation, and delineation of the tumour, but may also affect attenuation correction and overestimate the SUV values [53-55]**.**

Respiratory motion can decrease the SUV of a lesion located particularly the in the lower and middle lobes were the motion has a great impact and increases apparent the volume tumour volume. The SUV_{max} is more affected because it relies on the highest intensity voxel.

The blood glucose, insulin level, body size calculation and the time between injection and scanning can have a substantial impact on SUV. High levels of native glucose has a competitive impact of the FDG uptake resulting in an underestimation of SUV measurements. Insulin injection prior or close to the injection to FDG can increase the FDG transport mainly into the muscles and consequently reduce the FDG uptake in the target of interest.

Partial volume effect

The partial volume effect occurs when an object is two to three times smaller than the spatial resolution of the scanner and has a measured activity concentration that is less than the true concentration value. The spatial resolution is characterised by the PSF, which describes the image response to a point source. Partial volume effect affects images both qualitatively and quantitatively. The maximum value in the lesion will be lower than the true maximum value and the lesion appears to be larger than its real size. In PET/CT the PET and CT images shows this discrepancy very clearly (Figure 3).

The partial volume effect, consist of two phenomena [56]. The first effect is an image blurring produced by the PET imaging system. The spatial resolution in the PET images is limited by the detector design (e.g. by the crystal type and its sensitivity) and the reconstruction process [57]. The blurring results in a spill out from the small lesion to the surrounding tissue**.**

The second phenomenon is the image sampling. The radiotracer is sampled on a voxel grid. The contours of the voxel will not match the edge of lesion which results in that the voxels will include both the signal from the lesion and the background tissue. This effect is called the *tissue fraction effect*. The correction for PVE should account for both the resolution effect and the tissue fraction effect. (Figure 4).
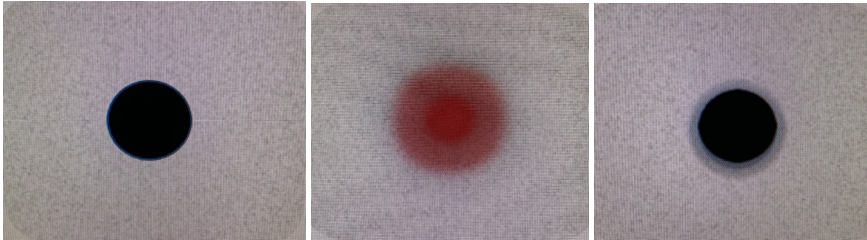
Figure 3. The impact of PVE. The actual lesion (left), lesion in PET (in the middle) image and lesion in CT image (right). The PVE is of lesser magnitude in the CT than in PET image.
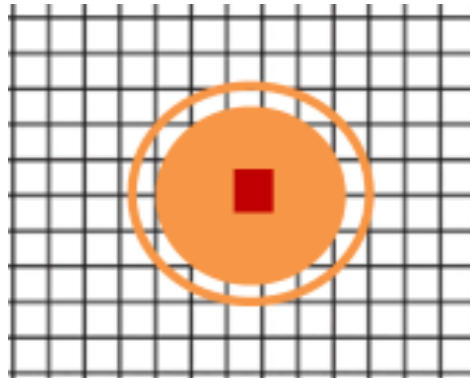
Figure 4. Tissue fraction effect. The red voxel shows the SUV with the highest SUV value. The VOI which include the lung lesion will also include surrounding tissue.

The compensation for PVE is difficult because the activity spills out from the tumour as well as it spills in from the surrounding tissue. Thus very often the spill in/spill out is not balanced which makes it difficult to predict the overall effect. The smaller the tumour the greater the underestimation (Figure 5). Small tumours will appear less aggressive than they are during follow up especially when they shrink in size and erroneously appear to have less activity than when it was larger [58].
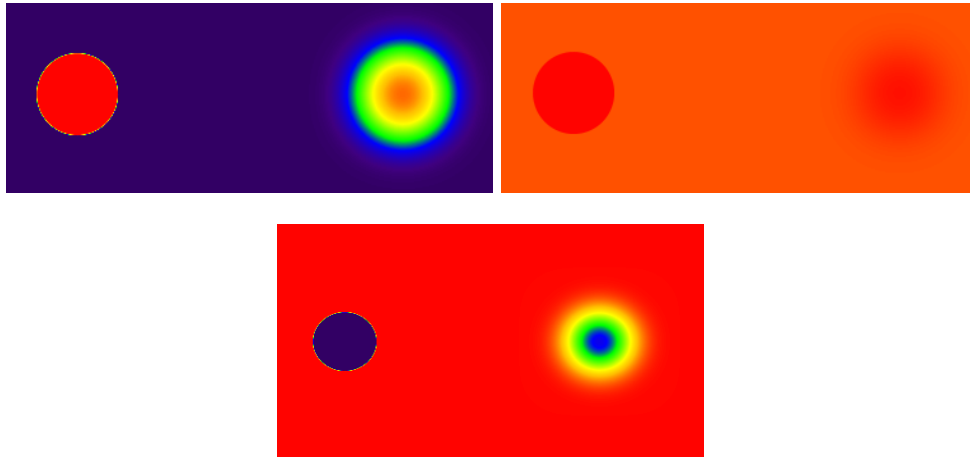
Figure 5. A. Spill-out from a high-activity area leads to reduced peak activity inside. **B** a small object and.spill-out and spill-in effects mostly cancel out, if radioactivity concentrations surrounding the object are similar **C.** If surrounding tissue has higher radioactivity concentration than the VOI, then spill-in (spill-over) leads to overestimated concentration inside the volume-of-interest.

Tumour

In addition the size and shape of the tumour also affect the PVE [56]. A tumour with a large surface area relative to its volume is more affected compared to solid tumours of same volume.

Surrounding Tissue

Spilling in depends very much on the surrounding background activity. A lung tumour will be less affected by spilling in than a tumour in the liver. The spill in can be difficult to estimate in particular when the tumour is surrounded by different tissues (e.g. heart, lung tissue, liver) [56]. Also when FDG uptake is measured during follow up the surrounding tissue can change from one scan to another.

The spatial resolution

The spatial resolution as aforementioned is partly determined by the canner features (crystal size and design 2 or 3D acquisition mode) but also on the reconstruction process. Spatial resolution determines how far the signal spreads around the actual location. High resolution gives a little spread whereas low resolution gives a large amount of spread [59].

Image sampling

The large pixels/voxels are the greater the chance of having a mixture of different tissues compared to small pixels/voxels. Using large voxels increases the risk of underestimating the metabolic activity of the tumour [56].

Applications of FDG measurements

Diagnosis

Tumour diagnosis and staging relies primarily on the qualitative interpretation of the FDG uptake [60]. Many cancers have an increased level of uptake and there can be overlap with that for inflammatory diseases. In attempt to discriminate benign diseases from malignancies, multiple SUV cut-off values have been proposed but no optimal value has been identified. One of the most commonly used thresholds during the early days of clinical use of FDG-PET/CT in evaluation of lung lesions was proposed by Fletcher et al. who suggested a cut-off SUV value of 2.5 to discriminate benign and malignant lesion. Many slow-growing malignant nodules demonstrate low FDG uptake as seen in sub-solid lung lesions, such as adenocarcinoma in situ, minimally invasive adenocarcinoma and adenomatous hyperplasia. In a study of sub-solid nodules, Chun et al. [61] found that inflammatory nodules had significantly higher SUV_{max} compared to malignant nodules. Despite the lack of a reliable cut-off value, FDG-PET/CT in selected patients can help to avoid unnecessary invasive procedures with small but existing mortality risk.

Prognosis

The PET data are not only for diagnosis, staging, response evaluation and detection of recurrence, but also for characterisation and prognostication. The biologic aggressiveness of a tumour plays a substantial role in the survival of cancer patient and the ability to predict the high-risk tumour can help to choose a better treatment strategy and may improve patient outcome. A study with lung cancer patients found that the baseline volumetric estimates, MTV and TLG are statistically significant prognostic indices and better than SUV_{max} and SUV_{mean} for prediction of patient outcome. This also applies for other cancers such as oesophageal cancer, thyroid cancer, head and neck cancer [45, 62]**.** However, the volumetric parameters are not used in standard clinical practice yet partly because the optimal segmentation method to measure these values has not been established.

FDG-PET/CT imaging in lung tissue and lung lesions

Quantification of static PET images of the lung remains challenging because of variations of the lung components during the respiration cycle. This work is focused on development of methodology and analyzing PET images in lung tissue and pulmonary nodules.

Tissue fraction effect

There are several factors can degrade the lung cell signal within a voxel. Respiratory motion influences the lung density whereas the gravity results in regional lung differences in density by increasing the blood component and decreasing the alveolar expansion. [63-66]. In addition, the variation of PET and CT signals between the respiratory cycles makes quantification in the lung even more difficult. The tracer concentration in the lung is sensitive to the amount of air content [13, 14]. An alveolus is approximately 6000 times smaller than a PET voxel [67]. Thus a single voxel will consequently contain a mixture of lung tissue, blood (approximately 10%-20%) and a large amount of air [14]. The measured activity concentration will correspond to the amount FDG in the different component and their fractions and not the signal from the parenchyma alone [68]. Several studies have already shown the importance of correction for air content in the lung [68-70]. Not accounting for air fraction can lead to inaccurate parameter estimates and misinterpretation.

Air fraction correction in static PET imaging
We assume that a lung voxel contains only two components, tissue (parenchyma and blood) and air and that there is a linear relationship between soft tissue density and Hounsfield units, where 1000 HU represents air.
In this context the lung parenchyma is regarded as a soft tissue with an X-ray absorption of 45 HU. The Hounsfield voxel within a CT voxel can be considered as the voxel fractional air volume (Va) obtained from the CT images:

$$V_a = \frac{HU_{voxel} - HU_{tissue}}{HU_{air} - HU_{tissue}}$$

The fractional tissue volume, as aforementioned is assumed to be proportional to the density of tissue in the voxel, and is given by: $V_t = 1 - V_a$

The air fraction corrected SUV (without air content) is then given by the measured SUV from the PET image divided by Vt [71].

$$SUV_{AFC} = \frac{SUV_{measured}}{V_t}$$

The accuracy of the AFC is very much dependent on the PET and CT voxels being perfectly matched, if not due to the respiratory motion, regions of e.g. fibrosis visualised on the CT will cause an under-correction of the PET if they correspond to normal appearing tissue during PET acquisition.

Intravenous contrast media and FDG-PET

Several studies have highlighted the value of combined anatomical and functional imaging [18]. The dual-modality PET/CT systems complement one another in diagnosis of malignant diseases. The use of IV contrast agent helps to identify pathologic changes in lesions appearing normal at unenhanced CT [72]. Some tumours, such as mucinous tumours, neuroendocrine tumours and adenocarcinoma in situ, do not reliably accumulate FDG but can be detected by aid of contrast-enhanced CT. Beyond all advantages with increased sensitivity and specificity using the additional contrast media during PET acquisition, there are some disadvantages that need to be addressed [73]. CT-based attenuation correction can lead to inaccuracies in the reconstructions of the PET images in the presence of contrast agents due to the high attenuation coefficients [53-55]. On the other hand, several studies have reported that the clinical impact of such attenuation correction differences seems to be small if the venous contrast medium phase are used for attenuation correction [74-77]. Plenty of contrast protocols for CT acquisition exist to assure imaging of different body regions. However, no consensus for the use of IV media exists and there is a considerable variation in protocols between institutions.

In addition to prevent mismatch in co-registration of PET and CT, which also has additional impact on the reconstruction and PET parameters, breathing protocols for CT acquisition have been implemented [78, 79].

Respiratory motion

Respiratory motion during PET acquisition is unavoidable, leading to two major confounding factors: misalignment between CT and PET imaging and reduced image quality of a lesion with significant blurring mainly the cranial-caudal direction in the lungs [80]. The movement of the lung results in overestimation of lesion volume in the PET image and an underestimation of radioactivity content [81-84] (Figure 5). In contrast to the PET image, CT represents a snapshot of a single part of the respiratory cycle. Due to misalignment, the attenuation corrected image may result in quantitative errors of activity concentration. Additionally small

lesions may be difficult to differentiate as the lesion contrast target-to-background ratio is reduced [85]. Several different methods have been employed to mitigate the respiratory motion artifacts during PET acquisition such as breath-holding, shallow breathing and respiration synchronized gating [86-91]. A previous study has shown that the extent of quantification error in the region of mismatch are not only due to the AC-map mismatch, but also on the tracer uptake surrounding the region of interest [78].

Respiratory motion can be corrected with gated acquisition [82, 83]. Respiratory gating has been achieved by defining the respiratory cycle and reconstructing the images (PET and CT) into small sections, bins of the range of amplitude (amplitude-based) [92] or breath cycle duration (phase-based gating) **[93]**. There are some disadvantages with respiratory gating. If a short phase of the respiratory cycle is selected, few counts are sampled and if it is long, there will still be motion artifacts in the image [94, 95]. A large study has shown a significant increase in volumetric values particularly in small pulmonary nodules if a partial volume algorithm was applied in gated PET/CT and ungated PET/CT [96].

Established external, hardware PET/CT gating is underutilized due to practical limitations (Figure 6). Newer developments with software gating, (data-driven gating), and BPL reconstruction with the new generation PET system allow improved image quality and quantification.

Respiratory gating may reduce motion artefacts but still fails to correct effect, PVE which most likely dominates over motion effects for small lesions [85]. Until now no feasible method for measuring volumetric parameters and accounting for the air fraction in clinical practice has been developed.
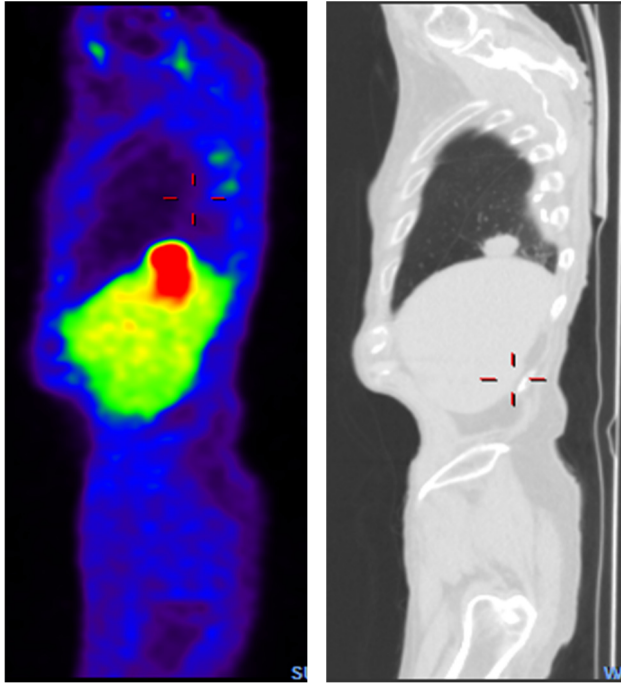
Figure 5. Impact of respiratory motion, namely smearing effect. The PET image shows an overestimated volume of the pulmonary nodule compared to the CT image.

Figure 6 Infrared camera mounted on the PET/CT table and an infrared reflective marker block that is fixed to the patient chest.

FDG-PET/CT imaging in COPD

COPD) is a major public health problem and causes morbidity and mortality. Accordingly to the World Health Organization COPD is the third leading cause of death were cigarette smoke is the major etiological factor beyond air pollution, smoke from biomass fuel and second-hand tobacco smoking. COPD is not restricted to the lungs but also a systemic manifestation associated with several comorbidities. Smokers with COPD are twice as likely to develop lung cancer compared to smokers without COPD [97]. There is consistent evidence that COPD and lung cancer share similar pathological mechanism, such as oxidative stress, inflammation, genetic pre-disposition and epigenetics [98]. The mechanism behind the systemic manifestation is not well understood but may be caused by overspill of the low grade inflammation from the lungs [99, 100]. There is still lack of understanding at the cellular, molecular and genetic level [101]. Small airway fibrosis and obliteration occur quite early in COPD. Therefore, it is important to understand the trigger mechanism that are switched on early in the disease.

Inflammatory cells, in particular activated neutrophils, macrophages and lymphocytes are known to have upregulated glucose metabolism, which means an increased FDG-uptake compared to non-activated counterparts [102]. Several studies for analyzing diffuse diseases with PET/CT describe the use of the Sokoloff compartment model [103] and Patlak [104] kinetic analyses, which represent the absolute quantification. Published studies of lung diseases (COPD and asthma) using dynamic ^{18}F-FDG-PET with attenuation scan using [68]Ge showed increased FDG uptake in patients with COPD compared to both normal and asthmatic subjects, but no difference between the latter two groups [9]. The authors concluded that ^{18}F-FDG-PET is a very promising tool for differentiating between these two diseases. Schroeder et al [105] found increased FDG uptake in sheep exposed to cigarette smoke and attributed this to the increased amount of activated neutrophils in the smoking lungs.

Studies have highlighted the potential use of ^{18}F-FDG as a highly reliable biomarker of neutrophilic inflammatory burden within the lungs [13] such as in widespread COPD and other lung diseases [1, 12, 15, 63], but there are some challenges though. The lung parenchyma with a density less than 1 g/mL differs from other organs in the body, containing lung air and blood which varies with the respiratory motion and the gravity dependent gradient. As aforementioned a PET voxel will therefore contain a large amount of air and a mixture of the other components [106]. In the supine position we will measure a higher activity concentration in the posterior and lower part of the lung [64, 66, 107]. This knowledge of confounding factors underlines the importance of correcting the measured activity concentration for lung inflation which was already shown in the 1980s and confirmed by Wollmer et al 1982 and Lambrou et al 2011. We hypothesised that inflammation in the airway in

current smokers can be detected with ^{18}F-FDG-PET/CT when correcting for air fraction to optimize quantification of FDG as an indicator of inflammation.

FDG-PET/CT imaging in pulmonary nodules

The evaluation of morphological and metabolic characteristics in small pulmonary nodules with little or no apparent ^{18}F-FDG accumulation pauses a challenging task in the in daily clinical practice. The underlying biology and uniformity of the lesions leading to a variation of SUV. Furthermore, respiratory motion as well as the impact of PVE on the SUV measurements results in an uncertainty in terms of quantification affecting diagnosis, staging and treatment monitoring. Distinguishing between benign and malignant small nodules is essential for appropriate investigation and further decision making. Quantification of a lesion´s metabolism is still based on visual and semi-quantitative evaluation, mainly with the widely used SUV max [34, 108, 109]. The magical threshold SUV max of 2.5 is a major source of concern, because it does not represent whole tumour activity concentration [38, 110]. The volumetric parameters, MTV and TLG have shown prognostic value in different malignancies particular in non-small cells cancer in advanced disease course, but not for diagnostic information and differentiation between malignant or benign lesion [48, 62, 111-114]. Determination of MTV and TLG still have limited use in clinical practice as both require accurate segmentation of the tumor. A further variable of potential interest is the tumor mass, as recent studies has shown that mass measurements of subsolid PN can enable detection of malignancy with less variability than volume and diameter measurements [115, 116].

Little attention has been given to facilitate quantification in the lung providing a vendor-independent method, usable in clinical practice. It is also of great importance to characterize the uncertainties in the estimated parameters due to the confounding factors such AFE and motion (mismatch between PET and CT).

Aims of the studies

The main objective of this thesis is to investigate and attempt to provide an approach for the most significant issues on PET image quantitation in the lung, namely the large amount of air and the density variations due to the respiratory cycle.

The methodology is shown through analysis of ^{18}FDG-PET/CT in phantom and patient data to produce reproducible parameters.

Specific aims

Paper I   To investigate whether current smokers have higher lung tissue uptake of ^{18}F-FDG than never-smokers when correcting for air fraction.

Paper II   To quantitatively determine if presence of IV contrast-enhanced PET/CT images influences the radiotracer concentration (SUV estimate) in the lung tissue compared to non-enhanced low-dose PET/CT images when both are compensated for the lung tissue density.

Paper III   To evaluate a new method for quantification of the mass and total metabolic activity in small solid and sub solid pulmonary nodules, including correction for partial volume effect.

Paper IV   To explore the accuracy of a new method (same method as in Paper III) for quantification of the total ^{18}F-FDG uptake, TLG in small sub- and solid lung nodules including correction for partial volume effect in respiratory ungated conventional static and gated ^{18}F-FDG-PET/CT.

Material and methods

Study design and populations

The Regional Ethical Review Board at Lund University and local Radiation Safety Board at Skåne University Hospital in Malmö approved all studies.

Paper I:

This was a retrospective study with 66 patients referred for a PET/CT examination for diagnosis or staging of cancer during 2010 to 2015. The patients were divided in two groups, 33 current smokers and a control group with 33 never-smokers, without any history of pulmonary disease and lesions (reported from patient notes). The control group was similar to the group of current smokers in terms of age and sex distribution. The smoking history and current smoking habits were recorded. The total tobacco consumption was expressed in pack years.

Paper II:

The study group consisted of 18 (5 men 13 women) prospectively included patients with known malignancy (5 with bladder cancer, 6 with malignant melanoma, 5 with colorectal cancer and 2 with gynaecological cancer). None of the patients had any history of known pulmonary disease (reported from patients notes), known lung metastasis, lung lesions or an ongoing radio- and chemotherapy. All patients gave their written informed consent to participate in this study. All PET examinations were done with a low-dose CT over the chest, immediately followed by an IV contrast enhanced diagnostic CT.

Paper III:

The study group consisted of 38 retrospectively included patients with small suspicious pulmonary malignancies who underwent ^{18}F-FDG-PET in combination with low dose CT at our institution between 2009-2015 and 2017-2018. The final diagnosis was established by histopathological examination or follow-up using CT. In addition, patient records were followed up. The following exclusion criteria were

applied: clinical suspicion of infection or interstitial lung disease, diabetes mellitus, previous radiotherapy, ongoing chemotherapy and heart failure. Prior to the examination an IV contrast-enhanced diagnostic CT not older than four weeks had been performed in all patients. During 2009-2015 most thoracic PET/CT scans were performed with IV contrast-enhanced CT and very few in combination with low dose CT. We therefore enlarged the study population with patients performed with FDG-PET in combination with low dose CT during 2017-2018.

Paper IV:

The study group consisted of 27 retrospectively included patients, (17 women and 10 men, range 43-87 years) with known or suspected malignant pulmonary lesions. We selected lesions located in the middle and lower lobes where the respiratory motion is assumed to have great impact on the quantification. The final diagnosis was established by histopathological examination or follow-up using CT. In addition, patient records were followed up. The PET scans were performed with ungated and gated PET over the chest in combination with a whole-body low radiation dose CT. For the gating we used a commercial software program Q.STATIC (GE Healthcare, Milwaukee, WI, USA).

Methods

PET/CT scan procedures and analysis

In **paper I** a standard PET/CT examination was performed after at least 6 hours fasting. The whole-body CT with intravenous contrast media was used for attenuation correction and was done in free breathing. The contrast enhanced scan was acquired during equilibrium late CT phase 70 s after administration of contrast media injection (during 2010-2015 most of the CT examination were routinely performed with i.v. contrast-enhanced diagnostic CT). The PET scanning consisted of imaging from the upper thighs to the base of the skull. The subjects were scanned in 5-7 bed positions using 2 min/bed position (Philips Gemini ToF 16 Philips Healthcare, Cleveland Ohio, USA). PET images with slice thickness of 4 mm were reconstructed in concordance with clinical routine using BLOB-OS-TF **(18)** OSEM reconstruction method with 3 iterations and 33 subsets. All PET images were evaluated based on qualitative visual assessment by one experienced nuclear medicine physician and the corresponding CT-images by one experienced radiologist. The readers were unaware of the smoking habits of the subjects.

The images were then loaded and analysed with a semiautomatic in-house software for segmentation (region growing-based), by an experienced radiophysicist (Figure

7). The right and left lung were segmented in the CT image, using a cut off value of -500 HU to avoid overlap of large pulmonary vessels and bronchi. The images were inspected and in individual cases adjusted to ascertain the artefactual uptake, such as thoracic wall, heart, the tip of the diaphragm and central airways, which were excluded from the analysis. The segmented lung VOI was then applied on the PET scan. The density of the lung was measured in HU and then converted into g/mL. The FDG uptake corrected for lung density was presented as mean SUV for

$SUV_{LD\ lung}$ and $SUV_{LD\ lung}$.

In **paper II** all examinations started with a non-enhanced low dose CT from the caudal part of the neck to the upper abdomen immediately followed by an IV contrast-enhanced diagnostic CT including the arterial phase of the chest and the upper abdomen and a whole-body scan in venous contrast medium phase. Both the low dose and IV ceCT were done during free breathing. The time from end of contrast injection to start of PET scanning was at least 1 minute, resulting in a well-mixed contrast medium in blood at the start of the PET scan. PET images with a slice thickness of 4 mm were reconstructed in concordance with clinical routine using BLOB-OS-TF **(18)** OSEM reconstruction method with 3 iterations and 33 subsets. All examinations were performed on Philips Gemini ToF 16.

Non-enhanced low dose CT and IV contrast enhanced late venous phase CT were used for attenuation correction giving two data sets based on the same set of raw PET emission data, resulting in one non-enhanced low dose PET/CT and one

IV ceCT PET/CT. Both data sets were also corrected for lung tissue fraction using the same in-house software as in paper I processed and analysed by an experienced radiation physicist. Comparison was performed between these two data of attenuation correction and correction for air fraction.
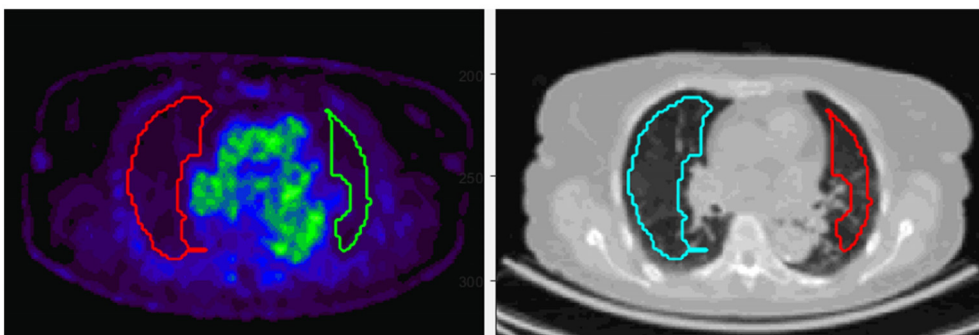
Figure 7. Segmentation of pulmonary tissue in CT image was performed with a region growing algorithm and placed on the PET image. Adjustment was done to ascertain that thoracic wall, central airways, the heart and the tip of the diaphragm were excluded from the analysis.

The method used in **paper III** was evaluated in phantom studies and applied in patients with PN. All patient studies were performed with a standard PET examination combined with low dose CT. Two different PET/CT scanners (Philips Gemini ToF 16 and Discovery MI GE) during two different time periods were included. Eighteen patients on the Philips system were scanned in 6-10 bed positions using 2 minutes/bed position and 144x144 matrix (pixel 4.0 x 4.0 x 4.0 mm). PET images with a slice thickness of 4 mm were reconstructed with CT derived attenuation correction using BLOB-OS-TF reconstruction method with OSEM (3 iterations 33 subsets). The acquisition of 20 patients during 2017-2018 were acquired on Discovery MI (GE Healthcare, Milwaukee, WI, USA) with the same preparation procedure as described above. The patients were scanned in 5-7 bed positions using 1.5 minutes/bed position and 256 x 256 matrix (pixel 2.7 x 2.7 mm^2 slice thickness 2.8 mm). Image reconstructions were performed according to routine clinical practice, using a Bayesian penalized likelihood reconstruction algorithm (Q.Clear) with a regularization factor, beta-value of 550 using time of flight and spread function modelling for recovery resolution [25, 27]. The acquired data were transferred to PACS (Picture Archiving and Communication System) for further processing and exported to an excel sheet containing the algorithm for the method.

In paper **IV** all examinations where performed on a SiPM-based PET-system, Discovery MI (GE Healthcare, Milwaukee, WI, USA) using the standard protocol for PET/CT. Patients were instructed to maintain a regular breathing pattern during the entire study. The examination session consisted of a scout view to define the scan volume from the base of the skull to the upper thighs both for the CT and PET. A low dose CT for attenuation correction and image analysis was acquired during free shallow breathing in 5-7 bed positions using 1.5 minutes/bed position with a matrix size of 256 x 256 matrix, a pixel size of 2.7 x 2.7 mm^2 and slice thickness 2.8 mm. The gated acquisition was performed over the thorax with 2-3 bed positions, 3 minutes/ bed position. The respiratory monitoring system, Motion Match, Q. static Real Time Position Management Varian Medical System, Palo Alto, CA, USA was used for gated acquisition. All patients were scanned in the arms-up position to obtain a good image quality. The PET images were reconstructed using a BSREM (Block-sequential regularized expectation maximization) Bayesian penalized likelihood reconstruction algorithm, (Q.Clear) with a beta value of 550 using time of flight and point spread function for recovery of true resolution [25, 27, 57]. As in study III the acquired data were transferred to PACS and analyzed similarly.

Method and algorithm used in Paper III and IV

The method was created to calculate the pulmonary nodule mass and the radionuclide activity adjusted for the spill in/out of the radioactive decay to and from the PN. When assuming that the surrounding structures are reasonable homogenous it is possible to account for and measure the contribution of background radioactivity. A VOI in the PET image large enough to include all the

annihilation events from a nodular lesion in the lung also incorporates radioactivity in the surrounding lung tissue. The volume of the pulmonary lesion, V_{VOIPET}, and the average SUV, $avSUV_{VOI}$, value are obtained in the PET image. The background activity is measured in a 2-3 mm wide space between two spheres outside the PN VOI.

The total radioactivity within the PN VOI = Volume of pulmonary lesion x average SUV), V_{VOIPET} x $avSUV_{VOI}$, contains radioactivity within the PN as well as in the in the background surrounding tissue SUV_{BG}

$$TLG_{PN} = V_{VOI,PET}\ avSUV_{VOI,PET} - (V_{VOI,PET} - V_{PN})avSUV_{BG}$$

The volume of PN (V_{PN}) is determined from the low dose CT applied for attenuation correction of the PET images.

Even if the spatial resolution of CT is superior to that of PET, blurring of the PN as a result of the respiratory motion of the lung creates an irregular shape of the PN which may contribute to uncertainty of the measurements. To overcome this issue there is an alternative approach similar to the one for measurements of SUV_{PN}. Assuming that there is a linear relationship between soft tissue density (D) and the absorbed X-rays measured in Hounsfield units (HU):

$$D = 1 + \frac{HU}{1000}$$

In this context, the PN is regarded as a soft tissue process with a X-ray absorption of 45 HU_{PN}, i.e. with a tissue density of 1.045 g/mL.

A VOI equal to V_{VOICT} encloses the PN with some margin. The mass density of PN is denoted by D_{PN} and $avHU_{CT}$ denotes the average Hounsfield units measured in V_{VOICT}. The V_{VOICT} also includes a background of surrounding tissue with volume equal to $V_{VOICT} - V_{PN}$ and an average of $avHU_{BG}$ measured in a separate VOI outside the V_{VOICT}.

The total mass of V_{VOICT} comprises of:

The mass of the PN denoted by M_{PN} with a volume M_{PN}/D_{PN}

The mass of background ($V_{VOICT} - M_{PN}/D_{PN}$) $(1 + avHU_{BG}/1000)$

$$M_{PN} = \frac{V_{VOI,CT}\ D_{PN}(avHU_{CT} - avHU_{BG})}{avHU_{PN} - avHU_{BG}}$$

$$V_{PN} = \frac{M_{PN}}{D_{PN}}$$

$$avSUV_{PN} = \frac{TLG_{PN}}{V_{PN}}$$

An estimation of the impact of the background in a lesion to lesion basis is obtained by using 4 additional spherical VOI: s outside the V_{PN} and increasing the radius with 2-3 mm and using the space between the spheres for background measurements and with a distance of at most 10 mm from V_{PN}. This results in 4 different values for each of M_{PN} and TLG_{PN} taking the mean value to characterise the PN and the standard error of the mean to represent the uncertainty of the values obtained.

Phantom study

We used a NEMA /IEC Body phantom to investigate the accuracy of our method in two separate sessions with a total of 11 irregular shaped tumor mimicking wall-less gelatin blobs. It should be noticed that gelatin blobs do not suffer from the disadvantage of standard spherical phantom inserts with hollow glass spheres, whose cold walls can have a strong impact on the measured partial volume effects [117] .

The activity concentration in the prepared blobs was aimed at approximately 5 and 20 kB/mL in the two sessions at the time of measurement (using 3 minutes and one bed position). This is close to the activity seen in pulmonary lesions in clinical studies (10-20 kBq/mL, with 1.5 minutes/bed position. The size of the blobs was in the range 0.3-1.5 mL (corresponding to spheres with diameters 9-14 mm). A larger blob (approx. 13 and 18 mL in the two sessions) was also prepared and scanned in each session, large enough to be used for measurements of activity concentration and density of the gelatin mix. The body phantom with a non-radioactive background consisted of sawdust with a mean CT density of some -840 HU, the reference mass of the tumor-mimicking blobs was measured on a balance (Mettler Toledo, Stockholm). Using this value, the reference radioactivity content of each blob was calculated from the radioactivity concentration and density of the gelatin mix. A SiPM-based PET-system, Discovery MI PET/CT system was used to acquire the images. Data were acquired for 3 minutes and one bed position with the gel blobs centred in the middle of the axial FOV. A scan protocol with a matrix size of 256 x 256, a pixel size of 2.7 x 2.7 mm^2 and a slice thickness of 2.8 mm was used. Image reconstructions were performed according to routine clinical practice, using a Bayesian penalized likelihood reconstruction algorithm (Q.Clear) with a regularization factor, beta-value of 550, time of flight and spread function modelling for recovery resolution [25, 27]. The acquired data were transferred to PACS (Picture Archiving and Communication System) for further evaluation and exported to an excel sheet containing the algorithm as aforementioned.

The PN-mimicking blobs in the phantom study were measured in the same way with the VOI technique as in the patient study. The radioactivity concentration and density of the large volume reference gelatine blob was measured in a large VOI and used in the calculation of TLG and volume of the smaller blobs. The evaluation was done by one reader.

All PET/CT images in the patient study were independently evaluated by two experienced nuclear medicine physicians and one reader with limited experience in nuclear medicine and no experience of PET/CT. Readings were transferred from PACS to an excel sheet for calculation of TLG_{PN} and M_{PN}.
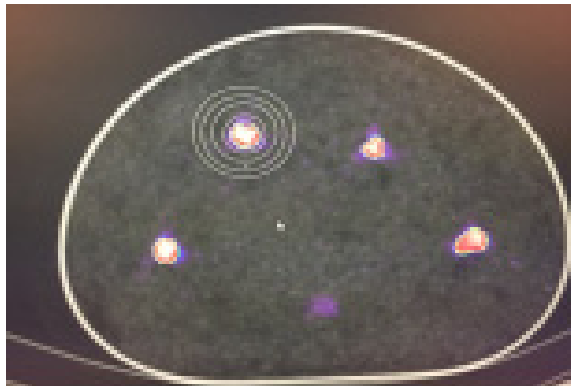
Figure 8 NEMA /IEC Body phantom with gelatine blobs. Four additional VOI:s were placed outside the V_{PN} for background measurements, resulting in 4 different values for each M_{PN} and TLG_{PN} and taking the mean to characterise the PN and the SEM to represent the uncertainty of the values obtained.

Respiratory gating

The respiratory gating system Q.STATIC, which is used in paper **IV,** is fully integrated in the whole-body PET protocol. The hardware consists of an infrared camera that is mounted on the PET/CT table and an infrared-reflective marker block that is fixed to the patient`s upper abdomen. The marker is visible to the camera during the whole acquisition (2-3 bed positions) over the chest. When activated, the system triggers the gated acquisition data to start at end-expiration. The software system then extracts a fraction of PET data from the end-expiratory part of the breathing cycle and forms a single PET image volume for review. This phase-based gating method has an ability to extract data during the quiescent expiration and to compensate for patient respiratory curve baseline drift. The conventional static PET, in contrast, uses the entire signal in each respiration cycle. Both the PET static and the Q.STATIC data are acquired simultaneously and reconstructed using the same reconstruction parameters. The reconstructed PET and CT images were transferred to PACS (Picture Archiving and Communication System) and to a customized

software developed for semiautomatic measurements NM Fusion module (by Sectra Imaging IT Solution AB, Linköping Sweden). The calculation methods for TLG_{PN}, $avSUV_{PN}$ and M_{PN} were calculated as previously described in paper III. In addition, the maximum SUV ($maxSUV_{PN}$) was recorded in the gated and ungated images. Since only one CT acquisition is performed, the same M_{PN} is used in the calculations of TLG_{PN} and $avSUV_{PN}$ in both the ungated and gated acquisitions.

Statistical analysis

In all papers a p-value of less than 0.05 was considered statistically significant. The analyses were conducted using IBM SPSS v 23-25, Armonk, NY.

Paper I

Objective test of the distribution was done with Shapiro-Wilk (S-W). Data from the two groups, smokers and never-smokers are presented as arithmetic means ± SD. Student's t-test and Mann Whitney U test were applied for comparisons. The correlation between lung density (HU), SUV corrected for air fraction SUV_{DL} (for the right and left lung), pack year and age were calculated as Pearson correlation and 95% confidence intervals in current smokers and never-smokers.

Paper II

Each patient generated two sets of attenuation corrected PET images over the chest: one with contrast media and one without. Due to the sample size and the non-normal distribution of the variables, Wilcoxon´s signed rank test was used to compare SUV resulting from calculations using low dose and IV contrast-enhanced CT as well as lung density.

Paper III and Paper IV

The distribution was evaluated with Shapiro-Wilks test. Mann-Whitney U test was used to test the differences between groups for the PET data. Results are presented as median and inter-quartile range (IQR) except where otherwise stated. Inter-reader agreement of measurements was calculated for M_{PN}, TLG_{PN} with the ICC (intraclass correlation coefficient) and was reported as a point estimate together with an estimate of 95% confidence interval (CI). Statistical significance was considered at $\alpha = 0.05$ level. The diagnostic performance of ^{18}F-FDG-PET based semi-quantitative analyses was assessed and receiver-operating characteristic (ROC) curves were calculated. Correlation was determined with the Spearman´s rank test. A significant correlation was defined when $p<0.05$. Bland-Altman was used for assessing comparability between measurements/methods.

Det tillhör sunt förnuft att välja en metod och pröva den.

Om den misslyckas, erkänn det ärligt och pröva en annan.

Men framförallt, pröva någonting.

      -Franklin D. Roosevelt

Results

Paper I

A total of 66 patient were included (32 women and 34 men). Mean age for never-smokers and smokers were 56±16 and 64±11 years, respectively. Current smokers were found to have a significantly higher (12.5%) SUV value (p<0.001) in the right lung and 8% (p=0.007) in the left lung compared with to the never-smokers when corrected for air fraction.
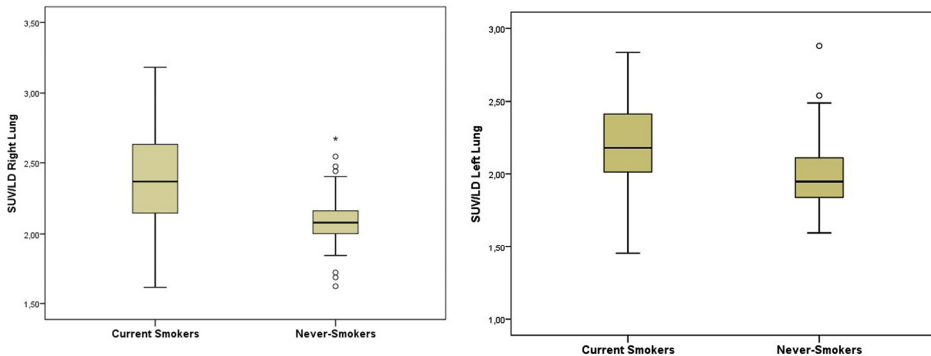

Figure 9. Medians and confidence intervals for mean SUV/LD in the lungs corrected for lung density in current smokers and never-smokers p< 0.05. The circles presented in never-smokers are outliers.

The current smokers had considerable total exposure to tobacco smoke, as indicated by a range in pack years from minimum 3 to 73 years. There was no statistically significant difference in blood glucose (p= 0.08), blood pool, (p=0.21), FDG uptake time (p=0.91) or lung density for the right and left lung (p= 0.91 and p= 0.80), between the two groups of subjects. Uncorrected SUV for the right and left lung, were numerically, but not statistically significantly, higher in smokers than in never-smokers. We found no correlation between pack years and ^{18}F-FDG uptake or lung density. When the CT was examined a number of subjects were noted to have emphysema therefore a subjective visual interpretation and grading of the extent was performed on the CT images. The interpretation showed signs of emphysema in 15 current smokers (10 with mild, 3 with moderate an 2 with severe emphysema) and only one never-smoker with mild emphysema.

Paper II

The mean age in the study population was 67.5±9 years. There were no apparent difference in the lung volume outlined in the two CT examinations. The mean attenuation of all CT data sets were converted into g/mL. As expected lung density was slightly higher in the IV ceCT than in the low dose CT (0.26±0.04 g/mL vs. 0.24±0.04 g/mL in the right lung and 0.26±0.05 g/mL vs. 0.24±0.05 g/mL in the left lung). Even if very small, the differences were statistically significant ($p<0.01$ for the right lung and $p<0.05$ for the left lung). SUV calculated without correction for tissue density was slightly, but statistically significantly higher when the i.v. ceCT was used for attenuation correction than when the low-dose CT was used (0.60±0.11 vs. 0.58±0.10 in the right lung and 0.55±0.09 vs. 0.52±0.11 in the left lung). When correction for tissue density was applied, there was no longer any significant difference between the two acquisitions (2.40±0.38 for ceCT vs. 2.45±0.39 for low-dose CT in the right lung and 2.20±0.33 vs. 2.28±0.37 in the left lung).
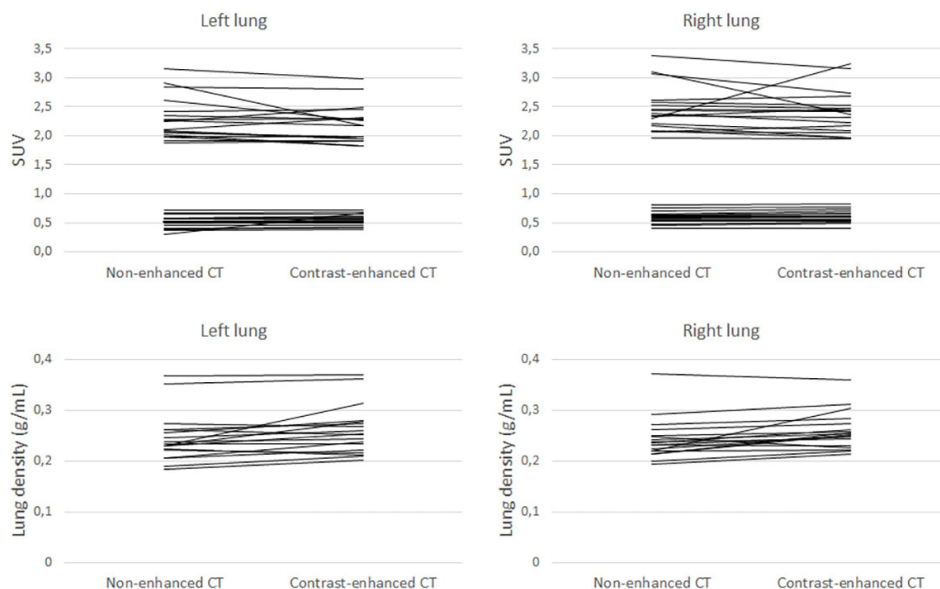

Figure 10. Individual measurements of SUV (upper panels) and lung density (lower panels) using non-enhanced and contrast-enhanced CT. SUV <1 represent data uncorrected for tissue fraction and SUV >1.5 data corrected for tissue fraction.

Paper III

Phantom study

A strong correlation was found between the measured blob mass, M_{blob} (measured on a balance) and calculated M_{blob}, and between the calculated total activity content and the reference blobs (r= 0.994 and r=0.998 P < 0.001 for both). There was a significant bias of weight (P=0.002) but no significant trend of difference (P=0.36). With respect of the radioactivity content there was significant bias (P=0.03) and a significant trend of difference (P= 0.013) of a minor 4% underestimation.

A   **B**
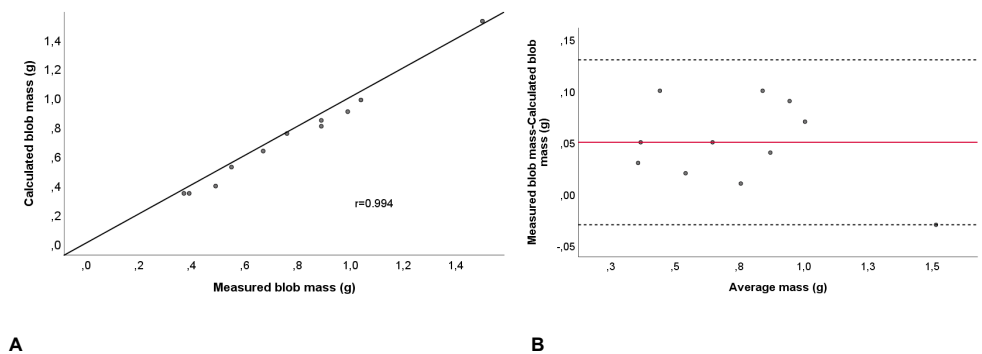
Figure 11. Phantom study. Correlation (**A**) and Bland-Altman plots (**B**) between the calculated mass of the blobs (g) vs. reference blobs, measured on a balance. The solid line in **A** is the line of identity. The solid line indicates the mean difference (0.05 g), whereas the dashed lines show the limits of agreement (-0.03 to 0.13 g)

A   **B**
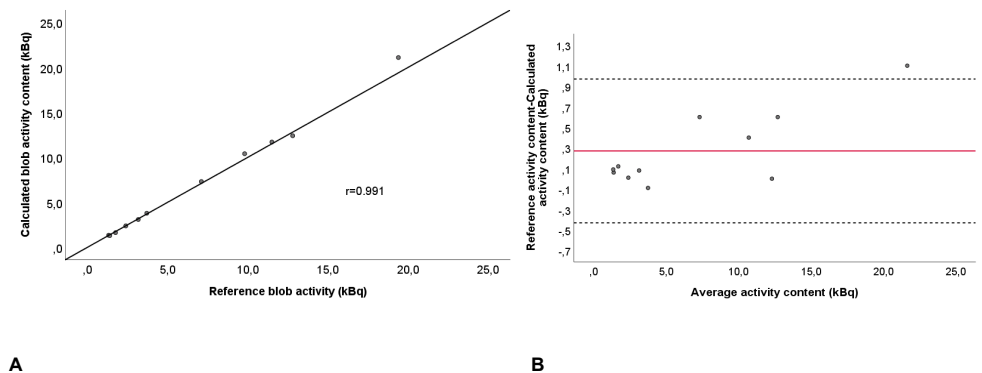
Figure 12. Correlation (**A**) and Bland-Altman plots (**B**) between the calculated blob activity content (kBq) vs. the activity content of the two reference blobs. The solid line in **A** is the line of identity. The solid line in **B** indicate the mean difference (0.27 kBq), whereas the dashed lines show the limits of agreement (-0.43 to 0.97 kBq).

Patient study

The clinical data are summarized in Table 1. There was no report about histopathological information or follow up in two patients. The calculated diameter of the pulmonary nodules expressed as median were 11 mm (9.2-12.7 mm)

The ICC between the three readers for TLG_{PN} and M_{PN} showed an excellent agreement, 0.994 (95% CI 0.997-0.999) and 0.999 (95% CI 0.998-0.999), respectively. The volume of VOI_{CT} was expressed as median and IQR was 2.9 (2.3-3.6) times larger than the volume of PN itself whilst volume of VOI_{PET} was 4.2 (3.5-6.5) times larger than $V_{PN.}$ Thus, a larger margin was required in the PET image compared to the CT image which is in line with respiratory movements and poor spatial resolution in the PET image. The correlation between the calculated volume of the pulmonary lesions, V_{PN} with the algorithm and volume measured with intravenous contrast enhanced CT values, IV $ceCTV_{PN}$ were strong ($r = 0.91$ *P* < 0.001*)*. The Bland-Altman analysis, of V_{PN} and IV $ceCTV_{PN}$ (Figure 13) is difficult to evaluate in terms of bias and trend of difference, due to both over- and underestimation of the pulmonary nodules in both methods. A great amount of the small pulmonary nodules, approximately < 2 mL show a difference of 40%.

There was a significant difference between benign and malignant lesions shown in (Table 3). The ability of $avSUV_{PN}$, TLG_{PN} and $maxSUV_{PN}$ to differentiate between malignant and benign lesions was described by ROC curves. AUC of TLG_{PN}, $maxSUV_{PN}$ and $avSUV_{PN}$ (Figure 14).

Table 1.

Clinicopathological variables	
Gender (n) men/women	11/27
Age	72.1 ± 10
Injected activity (MBq)	283 ± 52
Blood glucose (mmol/L)	6.2 ± 5.0
Accumulation time (min)	69 ± 5
Benign/Malignant pulmonary nodules	15/21
Histological type	
Adenocarcinoma	14
Squamous cell carcinoma	4
Metastasis*	3
Inflammatory lesion	2
Other benign lesions (follow-up without biopsy)	13

* 2 clear cell renal cell carcinoma, 1 rectal carcinoma
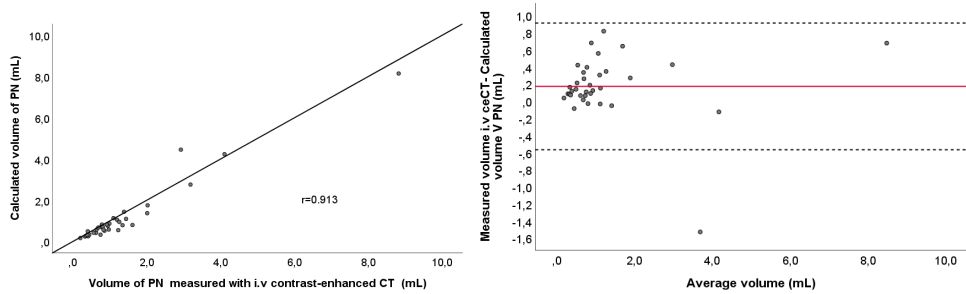
A   **B**

Figure 13. Correlation (**A**) Bland-Altman plot (**B**) of the volume, (mL) measured on i.v. contrast enhanced CT images (i.v. ceCTVPN) and the calculated volume of the pulmonary lesion VPN (mL). The solid line in A is the line of identity. The solid line in B indicates the mean difference (0.17 mL) whereas the dashed lines show the limits of agreement (-0.57 to 0.91 mL).

Table 2. Results of PN measurements presented as median and interquartile range. Mann-Whitney U test * p<0.05.

Variable	Benign lesions N= 15	Malignant lesions N= 21	*P* value
TLG$_{PN}$ (kBq/mL)	1.00 (0.55-3.10)	4.03 (2.13-5.98)	0.004
maxSUV$_{PN}$	1.41 (1.30-3.40)	2.92 (2.35-4.35)	0.006
avSUV$_{PN}$	1.78 (1.36-4.13)	5.06 (2.55-6.53)	0.004
M$_{PN}$ (g)	0.60 (0.34-0.86)	0.79 (0.52-1.75)	0.268
i.v ceCTV$_{PN}$ (mL)	0.91 (0.56-1.34)	0.90 (0.64-1.86)	0.620
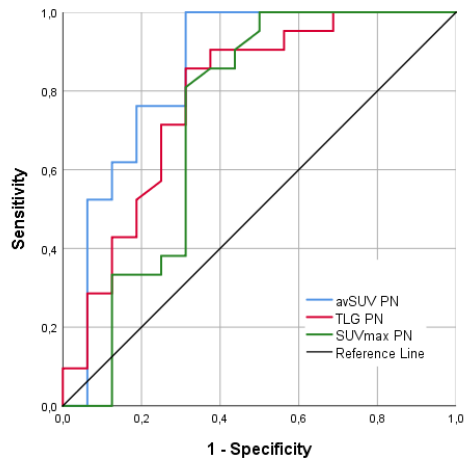
Figure 14. ROC characteristic curve analysis for avSUV$_{PN}$ (AUC 0.854 p<0.001) TLG$_{PN}$ (AUC 0.784 p=0.003) and maxSUV$_{PN}$ (AUC 0.729 p=0.018) in malignant lesions.

46

Paper IV

The patient characteristics and clinical details are summarized in Table 3. WE studied 27 patients. One patient was excluded due to lack of histopathological and follow up information. The variables TLG_{PN} in ungated and gated images showed a good correlation r=0.998. The Bland-Altman analysis between ungated and the gated images in terms of TLG_{PN} showed a mean difference 0.11 kBq and limits of agreement were -0.59 to 0.82 showing a slight trend of differences of 2.1%.There was no statistically significant difference in TLG_{PN} or $avSUV_{PN}$ between ungated and gated images (Table 4). As expected, $maxSUV_{PN}$ showed a highly significantly higher value (19 %) in the gated image. The M_{PN} remained unchanged between the two acquisitions due to the use of same low dose CT and therefore not reported in the Table 4.

Table 3. Patient characteristics and measurement conditions. Values are presented as mean and standard deviation.

Clinicopatological variables	
Gender (n) men/women	10/17
Age (years)	70.3 ± 11
Weight (kg)	72.7 ± 15
Injected activity (MBq)	288 ± 57
Uptake time (minutes)	61 ± 6
Blood glucose (mmol/L)	5.9 ± 0.7
Benign/Malignant pulmonary nodules	10/16
Histological type	
Adenocarcinoma	9
Squamous cell carcinoma	2
Angiosarcoma	1
Carcinoid	3
Metastasis (malignant melanoma)	1
Benign lesion (follow up with CT without biopsy)	10

*no histopathological or follow up information in one patient

Table 4. Results of ungated and gated PET image analyses expressed as median and interquartile range.

Variables	Ungated PET	Gated PET	*P* value
TLG_{PN} (kBq)	2.51 (1.15-9.89)	2.74 (0.94-10.20)	0.248
$avSUV_{PN}$	2.88 (1.32-5.86)	3.56 (1.41-5.36)	0.471
$maxSUV_{PN}$	3.27 (1.50-7.40)	3.97(1.29-8.60)	<0.001

Discussion

Main findings and interpretation in Paper I and II

Lung tissue and tissue fraction (air fraction)

Quantitative biases produced by attenuation and, to some extent, scatter can now be corrected. Other biases such as PVE are not routinely dealt with and overlooked in clinical practice. Different quantification approaches have been proposed, but no optimal method has been established to date. To improve the quantification in lung PET in clinical practice, validation of more feasible and non-vendor specific methods to account for tissue fraction effect is desirable. The findings in Paper I and II, show the importance of correcting for the air component, [13, 69, 118] in the lung images. The lung parenchyma, which is the only organ with a great amount of air content (expect the colon) has been wrongly interpreted. In clinical routine, common practice has overlooked that the SUV value in the lung has a different significance compared to solid tissues. By using the correction proposed in this study, the values will become analogue to that in e.g. the liver. We believe this correction to be a prerequisite for using PET to evaluate different diffuse lung diseases, e.g. interstitial lung diseases.

In paper I, we have shown that elevated uptake of ^{18}F-FDG in the lung tissue may be undetectable by reduced lung density if the activity concentration of the tracer is not corrected for air fraction. We found that the lung density in current smokers was only slightly lower than in never-smokers which may be explained by the fact that half of the smokers had developed some degree of emphysema [119]. Symptom-free current smokers with normal lung function can show a higher lung density compared to never-smokers which may reflect increased tissue density due to inflammation in smaller distal airways [3]. The higher uptake of ^{18}F-FDG in lung tissue in current smoker compered to never-smokers probably mirrors an inflammation response in the airways, due to enhanced active neutrophils.

In Paper II we focused on the influence of IV ceCT when correcting for both attenuation and the air component compared to non-enhanced low does CT. Several studies imaging pulmonary tissue have already demonstrated that the effect of contrast agent on the PET data is marginal in evaluation of patients with cancer [75-

77, 120, 121]. Looking at the lung tissue separately, the i.v. contrast media may affect the accuracy of attenuation correction by overestimating the attenuation and consequently overestimate the lung density and the SUV value. Using the proposed correction the relative error will be averaged out. Berthelsen et al, have shown that the presence of clinically relevant contrast media does not the significantly affect the 511 keV gamma rays. Our findings therefore, reflect the effect of contrast media on the CT examination. In our study, the air fraction correction with this correction method showed that the partial volume corrected average SUV increased by factor 4.2 for the right lung and 4 for the left lung compared to the original uncorrected SUV values which is in line with other studies [77].

Methodological issues and considerations

In Paper I, the average age in our study may have an additional impact on the results in the smokers, due to the age-associated changes in the respiratory and pulmonary immune system [122]. We also obtained very sparse information on symptoms or lung function in our subjects. Despite excluding subjects with clinical diagnosis of COPD, the population probably constituted a mixtures of subjects with normal lung function and subjects with some degree of air flow limitation, which is indicated of the high degree of emphysema. The PET/CT protocol was performed in accordance with the conventional time for detection 60 minutes (±10 min) which may not be the optimal time since the FDG uptake still can increase after that time-point. Despite these factors, a significant difference in SUV (corrected for lung density) was found in smokers even in subjects with emphysema. Our data support a previous study that have shown increased pulmonary uptake of ^{18}FDG in patients with COPD in combination with emphysema and provides a more convincing evidence. The investigators found an increased FDG in patients with COPD and emphysema but not in patients with AATD (α_1-antitrypsin deficiency) which shows that the two condition have different pathogenesis [123].

During the segmentation process of the PET images, using the same approach in both Paper I and Paper II there were some difficulties in identifying a distinct border in the peripheral part of the lung due to spillover from the chest wall, diaphragm and heart, which could have an impact on the SUV values. The analysis in the left lung was more complicated owing to its smaller size. In Paper II we used two CT data sets with attenuation correction on the same set of raw PET emission data, however, even with remaining contrast media during the PET acquisition, most of the contrast will be diluted when PET data are collected (in our study just over one minute after CT acquisition). A change in the PET/CT protocol may have been of interest, starting with the PET acquisition followed by the low dose and finally ending with IV contrast-enhanced CT to minimize any interference with the contrast agent

resulting in an eventual overestimation of SUV values. Another issue of consideration is whether our results are applicable to other PET/CT systems with different attenuation correction map using different scaling algorithms reconstruction algorithms and software.

In Paper I and Paper II, all measurements are results of an average ^{18}F-FDG uptake in the lung parenchyma, since we did not separately quantitate the amount of blood volume representing a large component (10-30%) of the PET voxel, adding to the PET signals. The amount of signals from the vascular system in our corrected SUV value varies with the respiration and the gravitation (non-dependent and dependent) in supine position. The proportion of blood, air, parenchyma, immune cells and fluid will change the contribution in terms of PET signals causing significant variability in different lung diseases.

Main findings and interpretation Paper III and IV

Method for delineation of lung lesions

Respiratory motion misalignment between transmission and emission scan have an impact on SUV values as well as PVE and AFE which results in limited PET signals in small nodules [56]. Volumetric parameters have shown a prognostic value in different malignancies in particular lung cancer. However, it is still challenging to define MTV accurately for heterogeneous lung nodules with low uptake and thus not universally applicable to all clinical scenarios due to inter- and intra-observer variability [124]. Several PET segmentation algorithms have been applied to FDG-PET images, such as threshold-based with fixed absolute, background, adaptive thresholds and algorithm-based methods [52, 125, 126]. These are mainly operator-specific and the measures dependent on image resolution, image noise and level of background activity. Another issue of interest is the tumour volumetry which have shown to be superior to diameter measurements in solid and subsolid nodules in terms and reproducibility and accuracy [115, 127]. Mass is a variable that integrates density and volume obtained from the CT data and increases if the volume or the density of the lung lesion increases [128].

In **Paper III** the major objective was to develop and evaluate of a new method for determination of total lesion glycolysis and calculate mass. The method also includes correction for the PVE, air fraction and the contribution of the variation of lung density.

We have chosen a different approach for determination of TLG_{PN}, which does not require an accurate segmentation of the PN which is the major advantage with this method. By placing a VOI large enough including all annihilation events from PN

and a part of the background tissue. By analysing this region enclosing the PN with some margin, many of the problems with PVE (the spatial resolution and the air content in lung tissue) and respiratory movements during PET acquisition can be mastered. The accuracy with this method relies mainly on the background activity and the X-ray absorption, representing the surrounding tissue enclosed in the VOI of the pulmonary nodule. It is therefore of great importance to acquire the variability for the individual patient depending on e.g. regional pulmonary disease.

Prior to the patient study the phantom study showed that our VOI technique is capable of measuring radioactivity and mass in the pulmonary lesion of different size with good and acceptable accuracy. The Bland-Altman analysis showed an underestimation of less than 0.05g i.e. 50 mg and 0.27 kBq for the activity content, without clinical significance. The patient study showed an excellent inter-observer agreement by three readers in assessment of TLG_{PN} and M_{PN}. One of the readers had no previous experience of PET/CT but got results comparable to the other two experienced readers.

The calculated mass of PN and the measured volume in the CT image showed a strong correlation, but the Bland-Altman showed both an over- and underestimation, especially in small PN <2mL and differences of 40%. One possible explanation of the findings is that the measured VOI of the PN in the CT image contained some air, due to the included surrounding tissue.

The differentiation between benign and malignant lesions by ROC curves showed a better discrimination in terms of TLG_{PN} and $avSUV_{PN}$ between benign and malignant lesion than SUV_{max}, but the material is too small for any firm conclusion and it should be noted, that this was not the scope of the study.

In order to reduce inaccuracies regarding quantification of PN in the middle and lower lobes due to respiratory motion in **Paper IV,** we evaluated the impact of the same method as in Paper III in ungated and respiratory gated PET/CT images.

Respiratory motion and its impact on quantification of PET parameters depends mainly on the distribution of the activity concentration in a volume that is larger than the real volume resulting in an underestimation. Liu et al have shown that the respiratory motion can lead to an underestimation of tracer concentration up to 30% or more and an overestimation in lesion volume by a factor of 2 or more[91]. Various methods have been used to reduce the motion artefacts and the mismatch between CT and PET images. Respiratory gated PET acquisition may reduce the motion artefacts but cannot correct for the partial volume effect which is most likely the prominent cause in small lesions[85].

The VOI in our method as aforementioned, encloses the entire lesion whether it has been moving or not.

We avoid not only the PVE but also the impact of respiratory motion. We did not find any significant difference between ungated and gated images in terms of

TLG$_{PN}$ or avSUV$_{PN}$ whereas maxSUV$_{PN}$ was higher in the gated image than in the ungated, as expected and in accordance with previous findings [129]. The Bland-Altman analysis showed a mean difference of 0.11 with a slight trend of difference (2%), which has no clinical impact. The results show that our calculated volumetric parameters seem to be less depended of the image resolution.

Methodological issues and considerations

The slight underestimation of M$_{blob}$ in the phantom studies could be explained by a slight diffusion of liquid from the blob into the sawdust in the phantom.

One of the drawbacks of metabolic imaging is that high FDG uptake is not specific for malignancies. Several studies already have shown that a perfect separation between benign and malignant PN cannot be achieved [130]. In fact active infectious and non-infectious inflammatory etiologies with abnormal ^{18}F-FDG uptake remain a major problem in the oncological setting [131]. Another concern is that, even if the tissue uptake is high in very small PN the SUV will be low due to the partial volume effect (spill out).

In this study we used two different PET systems which can have an impact on the max SUV$_{PN}$ value owing to the spatial resolution, noise and reconstruction process. However, looking at the two systems separately there was no significant difference in terms of TLG$_{PN}$ and avSUV$_{PN}$ as an indication that the method is applicable even when using different PET systems.

Similar to all other methods the analysis can be difficult to apply on lesions adjacent to the pleura, large blood vessels and large bronchi. Finally, an error shared by all segmentation methods is the error in attenuation correction due to the mismatch between low dose CT and PET. In Paper IV very small lesions may be misplaced, whereas somewhat larger lesions can be only partly overlapping resulting in an underestimation of lesion uptake and overestimation of background activity. Lesions close to the diaphragm may be affected by abdominal organs interfering with attenuation correction. This is on the other hand generally easily recognised in the images.

Conclusions

Paper I. We have found that current smokers have a higher lung tissue uptake of ^{18}F-FDG than in never smokers. Abnormal lung tissue uptake of ^{18}F-FDG in current smokers may be undetectable by reduced lung density if the uptake is not corrected for the air fraction. Furthermore, the higher activity concentration of the tracer in the lung tissue in current smokers compared to never-smokers is presumably due to increased numbers of activated neutrophils as an inflammation response in the airways.

Paper II. The study demonstrates on an intra-individual level that, use of i.v. contrast-enhanced CT for attenuation correction for lung parenchyma has only marginal effect on the assessment of ^{18}F-FDG uptake in the lung tissue, when removing the impact of the air fraction in the lung, using the same easy applicable method as in Paper I.

Paper III. The results show that the determination of total lesion uptake and mass of the pulmonary nodules do not require accurate segmentation of nodule. Good accuracy was demonstrated in a phantom study and excellent inter-observer agreement was found in patient studies. We conclude that this algorithm can overcome many of the confounding factors, PVE, respiratory motion and segmentation difficulties. This result should of course be considered preliminary requiring a confirmation in a larger group of patients to determine full potential and clinical impact.

Paper IV. In this study, we have shown that our new method for quantification of volumetric PET/CT parameters in small lung nodules gives similar results in ungated and respiratory gated studies. This indicates that the method is less dependent on the image resolution. The method reduces the problems owing to the partial volume and respiratory motion.

Numbers are free creations of the human mind that serve as a medium for the easier and clearer understanding of diversity of thought.

-Richard Dedekind (1831-1916) German mathematician

Future perspective

The results of the studies in this thesis raise further research and questions that must be addressed in the future.

Paper I and II, concerning different lung diseases: It opens opportunities for intervention studies in pathophysiological research, e.g. studies of the relation between inflammation and reduction of lung function, treatment and relation between inflammation and biomarkers in the blood. The finding of increased FDG uptake in smokers as a probable indication of increased activated neutrophils also offers the opportunity using FDG as an endpoint in preclinical studies.

The new methodology for determination of volumetric parameters derived from Paper III and IV could hopefully be used either for research or clinical purposes, e.g. for diagnosis or treatment monitoring due to its simplicity, reproducibility and independency of PET system. Despite promising primary results the method requires further validation to achieve more statistical confidence.

Finally, to confirm the described results from all the studies we need a larger dedicated patient sample study and clinical information, such as respiratory symptoms, spirometric data, inflammatory biomarkers, in- and outdoor exposure to noxious inhalants data from CT, lung tissue and lung lesion sampling to provide additional context for correct interpretation of PET quantification parameters.

Acknowledgments

Assocciate professor Sigrid Leide Svegborn for your never-ending friendly immeasurable support, valuable thoughts and explanation concerning physics during our lunches.

To my mentor *Karin Åström Olsson* MD PhD my very wise friend from the early years at Medical School in Göttingen, Germany, for all mental contribution and coaching. Always encouraging. Thank you for listening to my problems during this long research-travel, for our discussion about essentials of life but also for witty jokes, laughs, cooking and the annual traditional baking, lussekatter.

Kajsa Olsson MD, my colleague and friend for fruitful discussions and mental support dragging me through my toughest period during this work and not to forget all our pleasant lunches.

Nina Karindotter Borgendahl MD, for cooperation and coaching during our clinical workdays.

Lisa Hörberg MD and *Ingrid Jeppsson Swanberg* MD at the dept of radiology for all your support. It is always great to work together with you.

To all my wonderful *colleagues* for all your support, empathy and encouragement.

Finally, my husband *Ulf* and our two grown-up children *Erik and Marie,* you have been an enormous help pushing me through many short "dark tunnels" (ups and downs) and made me see the light behind. Thank you for understanding that I was not always mentally available.

Erratum

Paper 1

<u>Introduction,</u> Ref: Wollmer et al 1986 should *read 84*

<u>Discussion</u>, Ref: Wollmer et al 1986 should **read 84**, Density due to inflammation…… Wollmer et al 86 should **read 84** *(*Regional extravascular density and fractional blood volume of the lung in interstitial disease). Chen et al 2006 should **read *Hansson et al 1999***, [1] Hogg et al *The Nature of Small-Airway Obstruction in Chronic Obstructive Pulmonary Disease*
N Engl J Med 2004;350:2645-53.

<u>Conclusion</u> Ref: Brudin et al, should **read *Schroeder et al 1994*** *(PET Imaging of Regional 18F-FDG Uptake and Lung Function After Cigarette Smoke Inhalation)*

Manuscript 3

1. Page 10: read negligible bias, should read ***significant bias of both activity content and*** M_{blob}
2. Page 11: ROC curve analysis should read, ***AUC of*** TLG_{PN}***, 0.784 (P=0.003)***
3. Table 3: ***Only 36 patient*** *are reported, due to lack of histopathological information in two of the patients*
4. Page 12 read M_{blob} approximately 0.07g should read ***0.05g***

Manuscript 4

1. Page 5: "step and shoot" cine mode ***removed***
2. Page 7 Results: ….should read, ***with a diameter of 15 mm***
3. Page 8 : read independent, should read ***less dependent***
4. Page 9: read: "After background subtraction, the mass…. ***the mass is removed***
5. Page 9: should read ***underestimation of max*** SUV_{PN} ***in ungated images can be regarded a limitation.***
6. Figure 1: should read ***Bland-Altman analysis of TLG ungated/gated showed a mean diff of 0.11kBq and limits of agreement were -0.59 to 0.8.***
7. Table 2. M_{PN} ***is removed***
8. Tabell 1: ***one patient is excluded***
9. Figure 12, 15 should read ***kBq***

References

1. Hansson, L., et al., *Glucose utilisation in the lungs of septic rats.* Eur J Nucl Med, 1999. **26**(10): p. 1340-4.

2. Kaim, A.H., et al., *Autoradiographic quantification of 18F-FDG uptake in experimental soft-tissue abscesses in rats.* Radiology, 2002. **223**(2): p. 446-51.

3. Wollmer, P., et al., *Measurement of pulmonary density by means of X-ray computerized tomography. Relation to pulmonary mechanics in normal subjects.* Chest, 1986. **90**(3): p. 387-91.

4. Martinez, F.J., J.F. Donohue, and S.I. Rennard, *The future of chronic obstructive pulmonary disease treatment--difficulties of and barriers to drug development.* Lancet, 2011. **378**(9795): p. 1027-37.

5. Schuster, D.P., *The opportunities and challenges of developing imaging biomarkers to study lung function and disease.* Am J Respir Crit Care Med, 2007. **176**(3): p. 224-30.

6. Chen, D.L., et al., *Quantification of Lung PET Images: Challenges and Opportunities.* J Nucl Med, 2017. **58**(2): p. 201-207.

7. Groves, A.M., et al., *Idiopathic pulmonary fibrosis and diffuse parenchymal lung disease: implications from initial experience with 18F-FDG PET/CT.* J Nucl Med, 2009. **50**(4): p. 538-45.

8. Harris, R.S., et al., *18F-FDG uptake rate is a biomarker of eosinophilic inflammation and airway response in asthma.* J Nucl Med, 2011. **52**(11): p. 1713-20.

9. Jones, H.A., et al., *In vivo measurement of neutrophil activity in experimental lung inflammation.* Am J Respir Crit Care Med, 1994. **149**(6): p. 1635-9.

10. Madsen, P.H., et al., *Positron emission tomography in chronic obstructive pulmonary disease.* Hell J Nucl Med, 2013. **16**(2): p. 121-4.

11. Vaidyanathan, S., et al., *FDG PET/CT in infection and inflammation--current and emerging clinical applications.* Clin Radiol, 2015. **70**(7): p. 787-800.

12. Pantin, C.F., et al., *Measures of the inflammatory response in cryptogenic fibrosing alveolitis.* Am Rev Respir Dis, 1988. **138**(5): p. 1234-41.

13. Lambrou, T., et al., *The importance of correction for tissue fraction effects in lung PET: preliminary findings.* Eur J Nucl Med Mol Imaging, 2011. **38**(12): p. 2238-46.

14. Wollmer, P., C.G. Rhodes, and J.M. Hughes, *Regional extravascular density and fractional blood volume of the lung in interstitial disease.* Thorax, 1984. **39**(4): p. 286-93.

15. Chen, D.L., et al., *PET imaging approaches for inflammatory lung diseases: Current concepts and future directions.* Eur J Radiol, 2017. **86**: p. 371-376.

16. Klein, M., et al., *18F-fluorodeoxyglucose-PET/CT imaging of lungs in patients with cystic fibrosis.* Chest, 2009. **136**(5): p. 1220-1228.

17. Taylor, I.K., et al., *Imaging allergen-invoked airway inflammation in atopic asthma with [18F]-fluorodeoxyglucose and positron emission tomography.* Lancet, 1996. **347**(9006): p. 937-40.

18. Czernin, J., M. Allen-Auerbach, and H.R. Schelbert, *Improvements in cancer staging with PET/CT: literature-based evidence as of September 2006.* J Nucl Med, 2007. **48 Suppl 1**: p. 78s-88s.

19. Townsend, D.W., *Combined positron emission tomography-computed tomography: the historical perspective.* Semin Ultrasound CT MR, 2008. **29**(4): p. 232-5.

20. Anagnostopoulos, C., et al., *Assessment of myocardial perfusion and viability by positron emission tomography.* Int J Cardiol, 2013. **167**(5): p. 1737-49.

21. Gomperts, S.N., *Imaging the role of amyloid in PD dementia and dementia with Lewy bodies.* Curr Neurol Neurosci Rep, 2014. **14**(8): p. 472.

22. Gardner, S.F., et al., *Principles and clinical applications of positron emission tomography.* Am J Hosp Pharm, 1992. **49**(6): p. 1499-506.

23. Thomas, M.D., D.L. Bailey, and L. Livieratos, *A dual modality approach to quantitative quality control in emission tomography.* Phys Med Biol, 2005. **50**(15): p. N187-94.

24. Cal-González, J., et al., *Positron range estimations with PeneloPET.* Phys Med Biol, 2013. **58**(15): p. 5127-52.

25. Teoh, E.J., et al., *Phantom and Clinical Evaluation of the Bayesian Penalized Likelihood Reconstruction Algorithm Q.Clear on an LYSO PET/CT System.* J Nucl Med, 2015. **56**(9): p. 1447-52.

26. Thielemans, K., et al., *STIR: software for tomographic image reconstruction release 2.* Phys Med Biol, 2012. **57**(4): p. 867-83.

27. Tragardh, E., et al., *Impact of acquisition time and penalizing factor in a block-sequential regularized expectation maximization reconstruction algorithm on a Si-photomultiplier-based PET-CT system for (18)F-FDG.* EJNMMI Res, 2019. **9**(1): p. 64.

28. Surti, S., *Update on time-of-flight PET imaging.* J Nucl Med, 2015. **56**(1): p. 98-105.

29. Wang, X.Y., et al., *Comparison of different automated lesion delineation methods for metabolic tumor volume of 18F-FDG PET/CT in patients with stage I lung adenocarcinoma.* Medicine (Baltimore), 2017. **96**(51): p. e9365.

30. Hudson, H.M. and R.S. Larkin, *Accelerated image reconstruction using ordered subsets of projection data.* IEEE Trans Med Imaging, 1994. **13**(4): p. 601-9.

31. Valk, P.E., et al., *Whole-body PET imaging with [18F]fluorodeoxyglucose in management of recurrent colorectal cancer.* Arch Surg, 1999. **134**(5): p. 503-11; discussion 511-3.

32. Hounsfield, G.N., *Nobel Award address. Computed medical imaging.* Med Phys, 1980. **7**(4): p. 283-90.

33. Kinahan, P.E., B.H. Hasegawa, and T. Beyer, *X-ray-based attenuation correction for positron emission tomography/computed tomography scanners.* Semin Nucl Med, 2003. **33**(3): p. 166-79.

34. Kinahan, P.E., et al., *Attenuation correction for a combined 3D PET/CT scanner.* Med Phys, 1998. **25**(10): p. 2046-53.

35. Boellaard, R., et al., *FDG PET/CT: EANM procedure guidelines for tumour imaging: version 2.0.* Eur J Nucl Med Mol Imaging, 2015. **42**(2): p. 328-54.

36. Cheson, B.D., *Staging and response assessment in lymphomas: the new Lugano classification.* Chin Clin Oncol, 2015. **4**(1): p. 5.

37. Wahl, R.L., et al., *From RECIST to PERCIST: Evolving Considerations for PET response criteria in solid tumors.* J Nucl Med, 2009. **50 Suppl 1**: p. 122s-50s.

38. Ziai, P., et al., *Role of Optimal Quantification of FDG PET Imaging in the Clinical Practice of Radiology.* Radiographics, 2016. **36**(2): p. 481-96.

39. Im, H.-J., et al., *Current Methods to Define Metabolic Tumor Volume in Positron Emission Tomography: Which One is Better?* Nuclear medicine and molecular imaging, 2018. **52**(1): p. 5-15.

40. Zhuang, M., et al., *Variability and Repeatability of Quantitative Uptake Metrics in (18)F-FDG PET/CT of Non-Small Cell Lung Cancer: Impact of Segmentation Method, Uptake Interval, and Reconstruction Protocol.* J Nucl Med, 2019. **60**(5): p. 600-607.

41. Basu, S. and A. Alavi, *Feasibility of automated partial-volume correction of SUVs in current PET/CT scanners: can manufacturers provide integrated, ready-to-use software?* J Nucl Med, 2008. **49**(6): p. 1031-2; author reply 1032-3.

42. Kubota, K., et al., *Differential diagnosis of lung tumor with positron emission tomography: a prospective study.* J Nucl Med, 1990. **31**(12): p. 1927-32.

43. Sathekge, M.M., et al., *Dual time-point FDG PET-CT for differentiating benign from malignant solitary pulmonary nodules in a TB endemic area.* S Afr Med J, 2010. **100**(9): p. 598-601.

44. Nakajima, R., et al., *Prognostic Value of Metabolic Tumor Volume and Total Lesion Glycolysis on Preoperative 18F-FDG PET/CT in Patients With Renal Cell Carcinoma.* Clin Nucl Med, 2017. **42**(4): p. e177-e182.

45. Huang, Y.T., et al., *The prognostic value of fluorodeoxyglucose positron emission tomography metabolic tumor volume in solitary colorectal liver metastasis.* Asia Pac J Clin Oncol, 2017. **13**(5): p. e262-e270.

46. Hwang, S.H., et al., *Prognostic Value of Metabolic Tumor Volume and Total Lesion Glycolysis on Preoperative 18F-FDG PET/CT in Patients With Very Early and Early Hepatocellular Carcinoma.* Clin Nucl Med, 2017. **42**(1): p. 34-39.

47. Liao, S., et al., *Prognostic value of the quantitative metabolic volumetric measurement on 18F-FDG PET/CT in Stage IV nonsurgical small-cell lung cancer.* Acad Radiol, 2012. **19**(1): p. 69-77.

48. UyBico, S.J., et al., *Lung cancer staging essentials: the new TNM staging system and potential imaging pitfalls.* Radiographics, 2010. **30**(5): p. 1163-81.

49. Cheebsumon, P., et al., *Effects of image characteristics on performance of tumor delineation methods: a test-retest assessment.* J Nucl Med, 2011. **52**(10): p. 1550-8.

50. Spratt, D.E., et al., *Impact of FDG PET/CT on delineation of the gross tumor volume for radiation planning in non-small-cell lung cancer.* Clin Nucl Med, 2010. **35**(4): p. 237-43.

51. Tejwani, A., et al., *The role of PET/CT in decreasing inter-observer variability in treatment planning and evaluation of response for cervical cancer.* Am J Nucl Med Mol Imaging, 2012. **2**(3): p. 307-13.

52. Paulino, A.C. and P.A. Johnstone, *FDG-PET in radiotherapy treatment planning: Pandora's box?* Int J Radiat Oncol Biol Phys, 2004. **59**(1): p. 4-5.

53. Antoch, G., et al., *To enhance or not to enhance? 18F-FDG and CT contrast agents in dual-modality 18F-FDG PET/CT.* J Nucl Med, 2004. **45 Suppl 1**: p. 56s-65s.

54. Behrendt, F.F., et al., *PET/CT in lung cancer: Influence of contrast medium on quantitative and clinical assessment.* Eur Radiol, 2012. **22**(11): p. 2458-64.

55. Nakamoto, Y., et al., *Effects of nonionic intravenous contrast agents at PET/CT imaging: phantom and canine studies.* Radiology, 2003. **227**(3): p. 817-24.

56. Soret, M., S.L. Bacharach, and I. Buvat, *Partial-volume effect in PET tumor imaging.* J Nucl Med, 2007. **48**(6): p. 932-45.

57. Oddstig, J., et al., *Comparison of conventional and Si-photomultiplier-based PET systems for image quality and diagnostic performance.* BMC Med Imaging, 2019. **19**(1): p. 81.

58. Vesselle, H., et al., *Relationship between non-small cell lung cancer FDG uptake at PET, tumor histology, and Ki-67 proliferation index.* J Thorac Oncol, 2008. **3**(9): p. 971-8.

59. Boellaard, R., et al., *Effects of noise, image resolution, and ROI definition on the accuracy of standard uptake values: a simulation study.* J Nucl Med, 2004. **45**(9): p. 1519-27.

60. Schrevens, L., et al., *The role of PET scan in diagnosis, staging, and management of non-small cell lung cancer.* Oncologist, 2004. **9**(6): p. 633-43.

61. Chun, E.J., et al., *Differentiation between malignancy and inflammation in pulmonary ground-glass nodules: The feasibility of integrated (18)F-FDG PET/CT.* Lung Cancer, 2009. **65**(2): p. 180-6.

62. Lee, P., et al., *Metabolic tumor volume is an independent prognostic factor in patients treated definitively for non-small-cell lung cancer.* Clin Lung Cancer, 2012. **13**(1): p. 52-58.

63. Brudin, L.H., et al., *Regional lung density and blood volume in nonsmoking and smoking subjects measured by PET.* J Appl Physiol (1985), 1987. **63**(4): p. 1324-34.

64. Inoue, K., et al., *(18)FDG uptake associated with CT density on PET/CT in lungs with and without chronic interstitial lung diseases.* Ann Nucl Med, 2009. **23**(3): p. 277-81.

65. Robinson, P.J. and L. Kreel, *Pulmonary tissue attenuation with computed tomography: comparison of inspiration and expiration scans.* J Comput Assist Tomogr, 1979. **3**(6): p. 740-8.

66. Verschakelen, J.A., et al., *Differences in CT density between dependent and nondependent portions of the lung: influence of lung volume.* AJR Am J Roentgenol, 1993. **161**(4): p. 713-7.

67. Ochs, M., et al., *The number of alveoli in the human lung.* Am J Respir Crit Care Med, 2004. **169**(1): p. 120-4.

68. Holman, B.F., et al., *Improved correction for the tissue fraction effect in lung PET/CT imaging.* Phys Med Biol, 2015. **60**(18): p. 7387-402.

69. Win, T., et al., *Areas of normal pulmonary parenchyma on HRCT exhibit increased FDG PET signal in IPF patients.* Eur J Nucl Med Mol Imaging, 2014. **41**(2): p. 337-42.

70. Wollmer, P., et al., *Measurement of pulmonary erythromycin concentration in patients with lobar pneumonia by means of positron tomography.* Lancet, 1982. **2**(8312): p. 1361-4.

71. Cuplov, V., et al., *Issues in quantification of registered respiratory gated PET/CT in the lung.* Phys Med Biol, 2017. **63**(1): p. 015007.

72. Pfannenberg, A.C., et al., *Value of contrast-enhanced multiphase CT in combined PET/CT protocols for oncological imaging.* Br J Radiol, 2007. **80**(954): p. 437-45.

73. Cronin, C.G., P. Prakash, and M.A. Blake, *Oral and IV contrast agents for the CT portion of PET/CT.* AJR Am J Roentgenol, 2010. **195**(1): p. W5-w13.

74. Berthelsen, A.K., et al., *PET/CT with intravenous contrast can be used for PET attenuation correction in cancer patients.* Eur J Nucl Med Mol Imaging, 2005. **32**(10): p. 1167-75.

75. Bunyaviroch, T., et al., *Quantitative effects of contrast enhanced CT attenuation correction on PET SUV measurements.* Mol Imaging Biol, 2008. **10**(2): p. 107-13.

76. Mawlawi, O., et al., *Quantifying the effect of IV contrast media on integrated PET/CT: clinical evaluation.* AJR Am J Roentgenol, 2006. **186**(2): p. 308-19.

77. Yau, Y.Y., et al., *Application of intravenous contrast in PET/CT: does it really introduce significant attenuation correction error?* J Nucl Med, 2005. **46**(2): p. 283-91.

78. Goerres, G.W., et al., *PET-CT image co-registration in the thorax: influence of respiration.* Eur J Nucl Med Mol Imaging, 2002. **29**(3): p. 351-60.

79. Goerres, G.W., et al., *Accuracy of image coregistration of pulmonary lesions in patients with non-small cell lung cancer using an integrated PET/CT system.* J Nucl Med, 2002. **43**(11): p. 1469-75.

80. Pépin, A., et al., *Management of respiratory motion in PET/computed tomography: the state of the art.* Nucl Med Commun, 2014. **35**(2): p. 113-22.

81. Callahan, J., et al., *Motion effects on SUV and lesion volume in 3D and 4D PET scanning.* Australas Phys Eng Sci Med, 2011. **34**(4): p. 489-95.

82. Erdi, Y.E., et al., *The CT motion quantitation of lung lesions and its impact on PET-measured SUVs.* J Nucl Med, 2004. **45**(8): p. 1287-92.

83. Nehmeh, S.A. and Y.E. Erdi, *Respiratory motion in positron emission tomography/computed tomography: a review.* Semin Nucl Med, 2008. **38**(3): p. 167-76.

84. Liu, C., et al., *The impact of respiratory motion on tumor quantification and delineation in static PET/CT imaging.* Phys Med Biol, 2009. **54**(24): p. 7345-62.

85. Teo, B.K., et al., *The effect of breathing irregularities on quantitative accuracy of respiratory gated PET/CT.* Med Phys, 2012. **39**(12): p. 7390-7.

86. Changlai, S.P., et al., *Using Cine-Averaged CT With the Shallow Breathing Pattern to Reduce Respiration-Induced Artifacts for Thoracic Cavity PET/CT Scans.* AJR Am J Roentgenol, 2019: p. 1-7.

87. Grootjans, W., et al., *The Impact of Optimal Respiratory Gating and Image Noise on Evaluation of Intratumor Heterogeneity on 18F-FDG PET Imaging of Lung Cancer.* J Nucl Med, 2016. **57**(11): p. 1692-1698.

88. Thorndyke, B., et al., *Reducing respiratory motion artifacts in positron emission tomography through retrospective stacking.* Med Phys, 2006. **33**(7): p. 2632-41.

89. Gilman, M.D., et al., *Optimal CT breathing protocol for combined thoracic PET/CT.* AJR Am J Roentgenol, 2006. **187**(5): p. 1357-60.

90. Sun, T. and G.S. Mok, *Techniques for respiration-induced artifacts reductions in thoracic PET/CT.* Quant Imaging Med Surg, 2012. **2**(1): p. 46-52.

91. Liu, C., et al., *Quiescent period respiratory gating for PET/CT.* Med Phys, 2010. **37**(9): p. 5037-43.

92. Grootjans, W., et al., *Amplitude-based optimal respiratory gating in positron emission tomography in patients with primary lung cancer.* Eur Radiol, 2014. **24**(12): p. 3242-50.

93. Nehmeh, S.A., et al., *Four-dimensional (4D) PET/CT imaging of the thorax.* Med Phys, 2004. **31**(12): p. 3179-86.

94. Dahlbom, M., A. Kriszan, and J. Czernin, *SU-E-I-82: Image Signal-To-Noise Equalization in Whole Body PET Using Variable Acquisition Times.* Med Phys, 2012. **39**(6Part5): p. 3644.

95. Werner, M.K., et al., *Respiratory gating enhances imaging of pulmonary nodules and measurement of tracer uptake in FDG PET/CT.* AJR Am J Roentgenol, 2009. **193**(6): p. 1640-5.

96. Salavati, A., et al., *Application of partial volume effect correction and 4D PET in the quantification of FDG avid lung lesions.* Mol Imaging Biol, 2015. **17**(1): p. 140-8.

97. Brenner, D.R., J.R. McLaughlin, and R.J. Hung, *Previous lung diseases and lung cancer risk: a systematic review and meta-analysis.* PLoS One, 2011. **6**(3): p. e17479.

98. Eapen, M.S., et al., *Chronic Obstructive Pulmonary Disease and Lung Cancer: Underlying Pathophysiology and New Therapeutic Modalities.* Drugs, 2018. **78**(16): p. 1717-1740.

99. Sinden, N.J. and R.A. Stockley, *Systemic inflammation and comorbidity in COPD: a result of 'overspill' of inflammatory mediators from the lungs? Review of the evidence.* Thorax, 2010. **65**(10): p. 930-6.

100. Hogg, J.C., et al., *The nature of small-airway obstruction in chronic obstructive pulmonary disease.* N Engl J Med, 2004. **350**(26): p. 2645-53.

101. Soriano, J.B., F. Polverino, and B.G. Cosio, *What is early COPD and why is it important?* Eur Respir J, 2018. **52**(6).

102. Scherer, P.M. and D.L. Chen, *Imaging Pulmonary Inflammation.* J Nucl Med, 2016. **57**(11): p. 1764-1770.

103. Sokoloff, L., et al., *The [14C]deoxyglucose method for the measurement of local cerebral glucose utilization: theory, procedure, and normal values in the conscious and anesthetized albino rat.* J Neurochem, 1977. **28**(5): p. 897-916.

104. Patlak, C.S., R.G. Blasberg, and J.D. Fenstermacher, *Graphical evaluation of blood-to-brain transfer constants from multiple-time uptake data.* J Cereb Blood Flow Metab, 1983. **3**(1): p. 1-7.

105. Schroeder, T., et al., *Image-derived input function for assessment of 18F-FDG uptake by the inflamed lung.* J Nucl Med, 2007. **48**(11): p. 1889-96.

106. Rhodes, C.G., et al., *Quantitative measurement of regional extravascular lung density using positron emission and transmission tomography.* J Comput Assist Tomogr, 1981. **5**(6): p. 783-91.

107. Miyauchi, T. and R.L. Wahl, *Regional 2-[18F]fluoro-2-deoxy-D-glucose uptake varies in normal lung.* Eur J Nucl Med, 1996. **23**(5): p. 517-23.

108. McDonald, J.E., et al., *Assessment of Total Lesion Glycolysis by (18)F FDG PET/CT Significantly Improves Prognostic Value of GEP and ISS in Myeloma.* Clin Cancer Res, 2017. **23**(8): p. 1981-1987.

109. Sher, A., et al., *For avid glucose tumors, the SUV peak is the most reliable parameter for [(18)F]FDG-PET/CT quantification, regardless of acquisition time.* EJNMMI Res, 2016. **6**(1): p. 21.

110. Fletcher, J.W., et al., *A comparison of the diagnostic accuracy of 18F-FDG PET and CT in the characterization of solitary pulmonary nodules.* J Nucl Med, 2008. **49**(2): p. 179-85.

111. Chu, K.P., et al., *Prognostic value of metabolic tumor volume and velocity in predicting head-and-neck cancer outcomes.* Int J Radiat Oncol Biol Phys, 2012. **83**(5): p. 1521-7.

112. La, T.H., et al., *Metabolic tumor volume predicts for recurrence and death in head-and-neck cancer.* Int J Radiat Oncol Biol Phys, 2009. **74**(5): p. 1335-41.

113. Murphy, J.D., et al., *Postradiation metabolic tumor volume predicts outcome in head-and-neck cancer.* Int J Radiat Oncol Biol Phys, 2011. **80**(2): p. 514-21.

114. Tang, C., et al., *Validation that metabolic tumor volume predicts outcome in head-and-neck cancer.* Int J Radiat Oncol Biol Phys, 2012. **83**(5): p. 1514-20.

115. de Hoop, B., et al., *Pulmonary ground-glass nodules: increase in mass as an early indicator of growth.* Radiology, 2010. **255**(1): p. 199-206.

116. Scholten, E.T., et al., *Semi-automatic quantification of subsolid pulmonary nodules: comparison with manual measurements.* PLoS One, 2013. **8**(11): p. e80249.

117. Sydoff, M., et al., *Use of wall-less ^{18}F-doped gelatin phantoms for improved volume delineation and quantification in PET/CT.* Phys Med Biol, 2014. **59**(5): p. 1097-107.

118. Wollmer, P., et al., *Regional extravascular lung density and fractional pulmonary blood volume in patients with chronic pulmonary venous hypertension.* Clin Physiol, 1983. **3**(3): p. 241-56.

119. Torigian, D.A., et al., *In vivo quantification of pulmonary inflammation in relation to emphysema severity via partial volume corrected (18)F-FDG-PET using computer-assisted analysis of diagnostic chest CT.* Hell J Nucl Med, 2013. **16**(1): p. 12-8.

120. Berthelsen, A.K., et al., *PET/CT with intravenous contrast can be used for PET attenuation correction in cancer patients.* Eur J Nucl Med Mol Imaging, 2005. **32**(10): p. 1167-75.

121. Aschoff, P., et al., *Multiphase contrast-enhanced CT with highly concentrated contrast agent can be used for PET attenuation correction in integrated PET/CT imaging.* Eur J Nucl Med Mol Imaging, 2012. **39**(2): p. 316-25.

122. Lowery, E.M., et al., *The aging lung.* Clin Interv Aging, 2013. **8**: p. 1489-96.

123. Subramanian, D.R., et al., *Assessment of pulmonary neutrophilic inflammation in emphysema by quantitative positron emission tomography.* Am J Respir Crit Care Med, 2012. **186**(11): p. 1125-32.

124. Lin, Y., et al., *Prognostic value of preoperative metabolic tumor volumes on PET-CT in predicting disease-free survival of patients with stage I non-small cell lung cancer.* Anticancer Res, 2012. **32**(11): p. 5087-91.

125. Erdi, Y.E., et al., *Segmentation of lung lesion volume by adaptive positron emission tomography image thresholding.* Cancer, 1997. **80**(12 Suppl): p. 2505-9.

126. Graves, E.E., A. Quon, and B.W. Loo, Jr., *RT_Image: an open-source tool for investigating PET in radiation oncology.* Technol Cancer Res Treat, 2007. **6**(2): p. 111-21.

127. Kodama, K., et al., *Natural history of pure ground-glass opacity after long-term follow-up of more than 2 years.* Ann Thorac Surg, 2002. **73**(2): p. 386-92; discussion 392-3.

128. Marten, K., et al., *Inadequacy of manual measurements compared to automated CT volumetry in assessment of treatment response of pulmonary metastases using RECIST criteria.* Eur Radiol, 2006. **16**(4): p. 781-90.

129. Guerra, L., et al., *Respiratory gated PET/CT in a European multicentre retrospective study: added diagnostic value in detection and characterization of lung lesions.* Eur J Nucl Med Mol Imaging, 2012. **39**(9): p. 1381-90.

130. Khalaf, M., et al., *Relation between nodule size and 18F-FDG-PET SUV for malignant and benign pulmonary nodules.* Journal of hematology & oncology, 2008. **1**: p. 13.

131. Cheng, G., et al., *When should we recommend use of dual time-point and delayed time-point imaging techniques in FDG PET?* Eur J Nucl Med Mol Imaging, 2013. **40**(5): p. 779-87.

FACULTY OF MEDICINE

LUND
UNIVERSITY